The Spatiotemporal Transfer Function of the *Limulus* Lateral Eye

SCOTT E. BRODIE, BRUCE W. KNIGHT, and FLOYD RATLIFF

From the Rockefeller University, New York 10021

ABSTRACT The dynamics of the *Limulus* retina may be well described by the spatiotemporal transfer function, which measures the response of the eye to moving sinusoidal gratings. We consider a model for this system, which incorporates an excitatory generator potential, and self- and lateral inhibitory processes. Procedures are described which allow estimation of parameters for the model consistent with the empirical transfer function data. Transfer functions calculated from the model show good agreement with laboratory measurements, and may be used to predict accurately the response of the eye to arbitrary moving stimuli. The model allows convenient interpretation of the transfer function measurements in terms of physiological processes which underly the response of the *Limulus* retina.

INTRODUCTION

We have shown in the preceding paper (Brodie et al., 1978) that the response of the *Limulus* lateral eye to arbitrary time-varying patterns of illumination is well predicted by the methods of linear systems analysis. In the course of such analysis, the dynamic properties of the eye are incorporated into a function of spatial and temporal frequency, the eye's spatiotemporal transfer function. It follows that much of what can be learned of the eye's physiological properties through examination of its responses to light may be deduced from careful analysis of the measured transfer function.

The methods of systems analysis are indifferent to the nature of the processes which underly the relations between stimulus and response; it is precisely this independence of mechanism which gives these methods their great generality. In order to draw physiological conclusions from systems-analytic data, it is necessary to interpret the data by comparison with more direct studies of the underlying physiology. For example, it is reasonable to ascribe a feature of a measured transfer function to a certain physiological process only after the existence of the process has been established through direct investigation. In the context of a model suggested by mechanistic studies, the systems-analytic data can constitute significant evidence for the evaluation of physiological hypotheses. We have carried out such an investigation on the lateral eye of *Limulus*, a system whose physiology has been studied by both direct and indirect means for many years (for reviews, see Graham and Ratliff, 1974; Ratliff, 1974). In the present paper, we present the results of this study in terms of a general

model for the *Limulus* eye which has evolved from many separate investigations in our laboratory and in others.

MATERIALS AND METHODS

The analysis and experimental techniques used to measure the spatiotemporal transfer function $\mathcal{F}(\xi, \omega)$ of the *Limulus* eye are described in detail in the preceding paper (Brodie et al., 1978). Data were obtained from an *in situ* preparation of the *Limulus* lateral eye using cotton wick-silver/silver chloride electrodes to record activity in single optic nerve fibers (Hartline and Graham, 1932). The temperature of the animals was controlled by means of a constant-temperature circulator coupled to the animal via a modified ice bag (Brodie, 1978). Eye temperature was held at 22 ± 1/4°C.

In essence, the value of the transfer function at a spatiotemporal frequency pair (ξ, ω) is determined by the response of the eye to a stimulus consisting of a sinusoidal grating of spatial frequency ξ, modulated in counterphase fashion according to a sinusoidal temporal signal of temporal frequency ω. By virtue of the linearity of the system, the temporal sinusoid may be replaced by a signal consisting of a sum of several sinusoids, each at a different temporal frequency (Victor et al., 1977). This sum-of-sinusoids temporal signal is used in turn to modulate sinusoidal gratings of each of several spatial frequencies. The experimental protocol consisted of a periodic rotation through "analysis" episodes at each of eight spatial frequencies. Each episode lasted 150 s (60 s of illumination followed by 90 s for dark-adaptation); thus, each stimulus cycle of eight episodes lasted 20 min. The sequence was repeated until the preparation failed, typically after 6 or more h. (The moving-pattern "synthesis" episodes described in the previous paper were omitted from the protocol to maximize the number of analysis measurements obtainable from the preparation. This increased the signal-to-noise ratio of the transfer function measurements.) For one experiment, the analysis pattern was rotated 90° from the usual horizontal orientation to measure the distribution of the lateral-inhibitory coupling constants in the vertical direction.

Calculations were performed on a PDP 11/45 digital computer (Digital Equipment Corp., Maynard, Mass.) and displayed on a CalComp 565 incremental plotter (California Computer Products, Inc., Anaheim, Calif.). Calculations based on the measured transfer functions were implemented with the cubic spline interpolations described in the preceding paper. Model-based calculations were implemented with a library of FORTRAN complex-arithmetic subroutines.

THEORETICAL BACKGROUND

In this section, we summarize a model for the *Limulus* retina, which will serve to provide a context for the analysis of our transfer function measurements. Our objective is to obtain an explicit expression, in terms of model parameters, for the *Limulus* spatiotemporal transfer function, in a form suitable for direct comparison with our experimental measurements.

The basic organization of the *Limulus* retina may be summarized by the block diagram shown in Fig. 1 (Dodge, 1969). Light incident on the retina causes the production of an intracellular voltage change (the generator potential). Changes in the intracellular potential are also induced by the processes of self- and lateral inhibition. These voltages sum to produce a net intracellular potential, which serves as the input to the impulse-generating mechanism. The impulse generator produces the train of action potentials which are conveyed along the optic

nerve as the output of the retina. These nerve impulses themselves serve as input to the self- and lateral-inhibitory processes, which feed back into the retina. The steady-state response of this system is summarized by the Hartline-Ratliff equations (Hartline and Ratliff, 1957, 1958; Stevens, 1964; Knight et al., 1970):

$$r_m = \epsilon_m - K_s r_m - \sum_{n \neq m} k_{m \leftarrow n} \cdot (r_n - t_{m \leftarrow n})_+, \tag{1}$$

where r_m is the response of the m'th ommatidium, ϵ_m is the "excitation" of the m'th ommatidium (a function of the illumination incident on it), K_s is the self-inhibitory coupling constant, $k_{m \leftarrow n}$ is the coupling constant for the inhibitory effect of the n'th ommatidium on the m'th ommatidium, $t_{m \leftarrow n}$ is the threshold for this inhibitory effect, and the notation $(\ )_+$ indicates the piecewise-linear operator such that $(x)_+ = x, x \geq 0$; $(x)_+ = 0, x < 0$. We ignore the nonlinearity introduced by the dependence of inhibitory coupling on excitation (Lange,

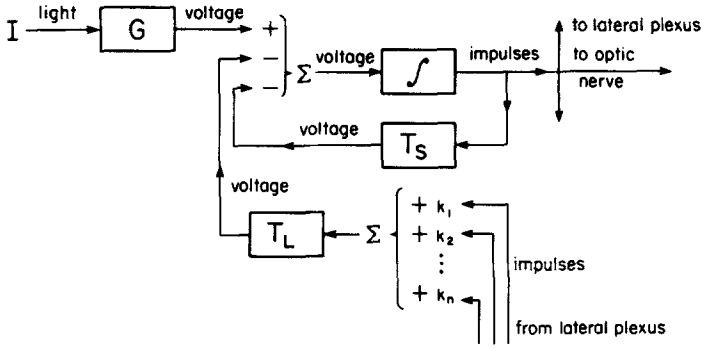

FIGURE 1. Block diagram of the *Limulus* retina. G denotes transduction from light to generator potential, $\int$ denotes the impulse generating mechanism, T_s denotes the self-inhibitory transduction, T_L denotes the lateral inhibitory transductions. Σ denotes summing points, where effects combine linearly, with signs as indicated.

1965; Barlow and Lange, 1974); in our situation, this effect does not appear to be significant.

The self-inhibitory feedback loop is not accessible to separate analysis in our input-output experiments. It is thus convenient to combine the impulse generator together with the self-inhibition into a single transduction, which we will refer to as the "encoder" (Fig. 2). With this convention, the Hartline-Ratliff equations take on an apparently simpler form:

$$r_m = e_m - \sum_{n \neq m} k_{m \leftarrow n} \cdot (r_m - t_{m \leftarrow n})_+, \tag{2}$$

where $e_m = \epsilon_m - K_s r_m$.

In the time-varying situation, the same block diagram applies, but the various quantities in the equations must be reinterpreted. First, we restrict attention to stimuli which cause all the ommatidia to fire impulses at a rate which fluctuates

about some mean operating level. As a rule, we assume that this operating level be chosen so that all ommatidia fire at a rate above their inhibitory thresholds. In such a regime, it is convenient to redefine the input and output variables to indicate the deviation from the mean value (of light intensity on input, of impulse rate on output), rather than the absolute numerical magnitude, of the stimulus or response. With these conventions, we may completely ignore the threshold terms in our equations (Ratliff et al., 1974).

We must also redefine the coupling coefficients so as to incorporate the dynamic aspects of the neural interactions which they represent. This is most simply accomplished by considering the response to signals which vary sinusoidally in time (Knight et al., 1970; Knight, 1973 *a*). By virtue of the linearity of the system, each portion of the visual transduction (generator potential, encoder, lateral inhibition) will respond to such an input with a sinusoidal output, according to its own transfer function. We represent the sinusoidal signals as (the real parts of) complex exponentials, and treat each stage of the

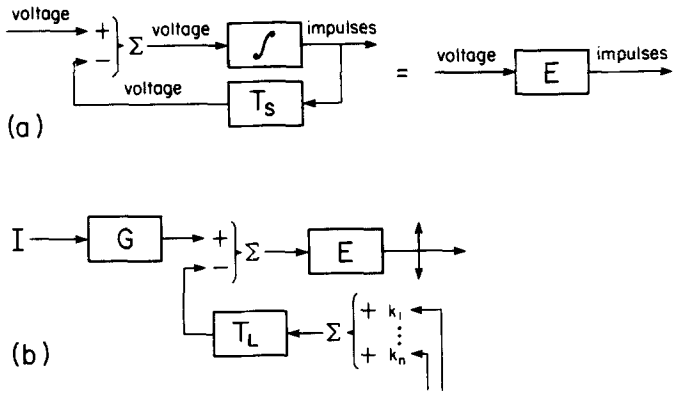

FIGURE 2. (*a*) Incorporation of the self-inhibitory feedback loop and impulse-generating mechanism into a single encoder transduction, *E*. (*b*) Simplified block-diagram of *Limulus* retina.

visual transduction in turn. First, we consider the excitatory component of the generator potential:

$$\epsilon_m(t) = G(\omega) I_m e^{i\omega t}, \tag{3}$$

where $G(\omega)$ is the light-to-generator-potential transfer function, and $I_m e^{i\omega t}$ is the illumination incident on the m'th ommatidium. The net intracellular potential V_m is the sum of this excitation and the total lateral inhibition:

$$V_m(t) = \epsilon_m(t) - T_L(\omega) \cdot \sum_{n \neq m} k_{m \leftarrow n} r_n(t). \tag{4}$$

This equation has been written so as to incorporate the experimental observation (Ratliff et al., 1974) that all the inhibiting ommatidia show the same temporal transfer function for lateral inhibition, which we denote $T_L(\omega)$. (In Eq. 4, $V_m(t)$

and $r_n(t)$ are functions of time proportional to $e^{i\omega t}$.) Finally, the impulse-train output is related to the net potential V_m according to the formula:

$$r_m(t) = E(\omega)V_m(t), \tag{5}$$

where $E(\omega)$ is the transfer function of the encoder, including impulse generation and self-inhibition. Because, in our experiments, the intracellular potential V_m is not accessible to direct measurement, it is convenient to use the steady-state impulse rate of the m'th ommatidium as a measure of this potential. With this choice of units for V_m, we may treat the encoder transfer function $E(\omega)$ as a dimensionless quantity. Eqs. 3–5 can be combined to obtain a dynamic equation analogous to the static Eqs. 1 and 2:

$$r_m(t) = E(\omega)[G(\omega)\cdot I_m e^{i\omega t} - T_L(\omega)\cdot \sum_{n\neq m} k_{m\leftarrow n} r_n(t)]. \tag{6}$$

The relation (Eq. 6) is an explicit inhomogeneous set of simultaneous linear equations which may be solved for the $r_m(t)$ in terms of the stimulus pattern I_m. For our purposes, however, it is more convenient to work instead with a continuous version of this system (Kirschfeld and Reichardt, 1964). To this end, we restrict our attention to stimuli which vary in space only along the x-axis (and thus, at any time t, are constant along vertical lines), and assume that each ommatidium in a given vertical column responds in the same way to such a stimulus. (This last assumption is made only for reasons of computational convenience; a more detailed treatment is discussed in the Appendix.) We may now replace the discrete index m with the continuous variable x, the horizontal coordinate along the eye. With this notation, Eq. 6 may be replaced by a corresponding integral equation:

$$r(x, t) = E(\omega)[G(\omega)I(x)e^{i\omega t} - T_L(\omega)\int k(x - u)r(u, t)\mathrm{d}u], \tag{7}$$

where we have incorporated the experimental observation that, at least away from the edges of the eye, the inhibitory coupling between two (vertical strips of) ommatidia depends, to a good approximation, only on the distance between them (Barlow, 1969). In other words, the inhibitory kernel takes the translation-invariant form $k(x, u) = k(x - u)$.

To obtain the spatiotemporal transfer function from Eq. 7, we take as input a sinusoidal grating $I(x) = e^{i\xi x}$. The response to such a sinusoidal input must be a sinusoidal signal of the form $r(x, t) = \mathcal{F}(\xi, \omega)e^{i(\xi x+\omega t)}$, where $\mathcal{F}(\xi, \omega)$ is, by definition, the spatiotemporal transfer function of the system. We have

$$\begin{aligned}
\mathcal{F}(\xi, \omega)e^{i(\xi x+\omega t)} &= E(\omega)[G(\omega)e^{i(\xi x+\omega t)} \\
&\qquad - T_L(\omega)\int k(x - u)\,\mathcal{F}(\xi, \omega)e^{i(\xi u+\omega t)}\mathrm{d}u] \\
&= e^{i(\xi x+\omega t)}E(\omega)[G(\omega) - T_L(\omega)\mathcal{F}(\xi, \omega)\int k(u)e^{-i\xi u}\mathrm{d}u] \qquad (8)\\
&= e^{i(\xi x+\omega t)}E(\omega)[G(\omega) - T_L(\omega)\mathcal{F}(\xi, \omega)\tilde{k}(\xi)],
\end{aligned}$$

where $\tilde{k}(\xi) = \int k(u)e^{-i\xi u}du$ is the Fourier transform of the inhibitory kernel. Eq. 8 may be solved readily for $\mathcal{F}(\xi, \omega)$, yielding the expression:

$$\mathcal{F}(\xi, \omega) = \frac{E(\omega)G(\omega)}{1 + E(\omega)T_L(\omega)\tilde{k}(\xi)}. \tag{9}$$

It is necessary to make one correction to the idealized transfer function of Eq. 9, to account for the limited resolving power of the *Limulus* optics. The derivation above assumes that the eye, in effect, is a perfect continuum of visual receptors, each excited only by illumination at exactly one x-coordinate. The effect of our imperfect stimulus optics and the finite size of the ommatidial light-collectors may be accounted for by convolving the stimulus with an effective "point spread function," $P(x)$, and using this degraded stimulus as the input $I(x)$ in Eq. 7. The equivalent correction in the frequency domain is the multiplication of the spatiotemporal transfer function by the Fourier transform of the point-spread function, which we denote by $\tilde{P}(\xi)$.[1] It is also convenient to include a real parameter M, to adjust the absolute magnitude of the complete transfer function. This constant subsumes several proportionality constants which are implicit in the component transfer functions, but which cannot be separately determined from our measurements of the response of the whole eye. We thus obtain the final form:

$$\mathcal{F}(\xi, \omega) = \frac{M \cdot \tilde{P}(\xi)E(\omega)G(\omega)}{1 + E(\omega)T_L(\omega)\tilde{k}(\xi)}. \tag{10}$$

The model of the *Limulus* visual system summarized by Eq. 10 is based, in essence, on the notion of recurrent mutual lateral inhibitory interaction first described in the original Hartline-Ratliff equations. Accordingly, we will refer to Eq. 10 as the Hartline-Ratliff model for the *Limulus* spatiotemporal transfer function.

We now consider in turn the various transductions $\tilde{P}$, E, G, T_L, and $\tilde{k}$, which enter into the Hartline-Ratliff model transfer function (Eq. 10). For each transduction, we obtain an explicit expression for the corresponding transfer function, in terms of parameters describing more basic aspects of the underlying physiology. Our ultimate goal in this paper is to determine values for these parameters, and thus further refine our physiological description of the *Limulus* eye.

We begin with $G(\omega)$, the transfer function from light to generator potential. This transduction may be studied directly in excised preparations by impaling the *Limulus* eccentric cell with a microelectrode and measuring the changes in intracellular potential induced by flickering light (Purple, 1964; Pinter, 1966; Dodge et al., 1968; Knight et al., 1970). Data obtained in this way have been well accounted for by the "adapting-bump model" (Rushton, 1961; Dodge et al., 1968; Knight, 1973*c*; Wong, 1977).[2] This model is motivated by the observation that, at low light levels, the generator potential is clearly resolved into a sequence of small discrete depolarizations ("bumps") which increase in fre-

[1] In the field of optics, the function $\tilde{P}(\xi)$ is known as the "spatial modulation transfer function."

[2] Wong, F., B. W. Knight, and F. A. Dodge. 1978. Dispersion of latencies and the adapting-bump model in *Limulus* photoreceptors. Manuscript in preparation.

quency, but which decrease in size ("adapt") as the incident illumination increases. On the basis of a few statistical and physiological assumptions, these considerations lead to an explicit form for the generator potential transfer function:

$$G(\omega) = e^{-i\omega t_l} \cdot \left(\frac{i}{1 + it_d\omega}\right)^{n_d} \cdot \left(\frac{1}{1 + it_b\omega}\right)^{n_b} \cdot \left(1 - \frac{R}{1 + t_a\omega}\right) \cdot \left(\frac{it_a\omega}{1 + it_a\omega}\right)^{p}. \quad (11)$$

The factor $e^{-i\omega t_l}$ is a pure phase-lag introduced by the finite delay ("latency") between the absorption of incident photons and the occurrence of the bumps they produce; t_l is the mean delay. The next factor $1/(1 + it_d\omega)^{n_d}$ describes the effect of stochastic variation of this latency interval about its mean. Here, the distribution of latencies is approximated by a gamma-density with parameters t_d and n_d. This corresponds, in the frequency domain, to the factor indicated (Wong, 1977). The third factor, $1/(1 + it_b\omega)^{n_b}$, expresses the dependence of the transfer function on the bump shape, which is modelled as a gamma-density with parameters t_b and n_b.

The last two factors in Eq. 11 describe the adaptation of the generator potential. As may be seen from direct measurements of the light-to-generator potential transduction (for example, Dodge et. al., 1968), this adaptation occurs on two different time scales. At very low frequencies, the dynamics show a frequency response proportional to $(i\omega)^p$ (Biederman-Thorson and Thorson, 1971; Thorson and Biederman-Thorson, 1974). At higher frequencies, there is a stronger dependence on frequency, which we have modelled, after the "minimal model" of Knight (1973 *c*), as a high-pass filter $(1 - R/[1 + it_a\omega])$. Here, t_a is a time constant which specifies the frequency region over which this adaptation effect occurs, and R describes the magnitude of the adaptation effect in this frequency region. We have adopted the form $[it_a\omega/(1 + it_a\omega)]^p$ to describe the very low frequency adaptation effect in such a way as to make a gradual transition to unity, centered around the characteristic frequency $\omega = 1/t_a$.

We consider next $E(\omega)$, the transfer function for the encoder, which includes the impulse-generating mechanism and a self-inhibitory feedback loop. The precise form of this function depends on the choice made for the variable which describes the output of the encoder. For reasons of simplicity and compatibility with experimental data, we shall use the "mean impulse density" function, $r(t)$, as described in the previous article (Brodie et al., 1978). Such encoders have been described in great detail (Knight et al, 1970; Barbi et al., 1975; Fohlmeister et al., 1977 *a*), but for our purposes, a simplified model will suffice. First, we assume that the impulse-generating mechanism is adequately described as a simple "integrate-and-fire" device, which produces a nerve impulse whenever the running integral of the input voltage reaches a criterion value; the integral is reset to zero after each impulse is fired (Knight, 1973 *b*). An important property of such an encoder is that, if mean impulse density is taken as the output variable, then the encoder produces an output which is a perfect replica of the input (Knight, 1972). In other words, the transfer function of the impulse generator is the constant 1. The transfer function $T_s(\omega)$ for the self-inhibitory transduction cannot be measured directly, but it may be deduced from measurements of the self-inhibitory impulse response seen in the intracellular potential after the occurrence of a neural impulse (Purple, 1964; Stevens, 1964; Dodge,

1969). This inhibitory transient may be modeled accurately as a single exponential decay of the form $\kappa e^{-t/\tau}$, where κ describes the strength of the self-inhibitory effect, and τ is the time constant for the decay. This impulse response corresponds to the transfer function

$$T_s(\omega) = \frac{\kappa}{1 + i\tau\omega}. \tag{12}$$

Note that in Eq. 12 we have incorporated the self-inhibitory coefficient κ into the function T_s.

In a neural encoder with self-inhibition, the inhibitory transients occur as discrete events, phased to the occurrence of impulses in the encoder output. This discrete aspect of the inhibitory process is reflected in subtle features of the corresponding transfer function for the encoder (Knight et al., 1970; Shapley, 1971). As these features occur mainly at frequencies greater than the mean impulse rate, we may safely ignore them in our analysis. With this simplification, we may regard the encoder as an ordinary (continuous variable) linear system with feedback (Fig. 2 *a*). We thus immediately obtain the relation

$$E(\omega) = 1 - E(\omega) \cdot T_s(\omega). \tag{13}$$

Solving for $E(\omega)$ yields

$$E(\omega) = \frac{1}{1 + T_s(\omega)} = \frac{1}{1 + \dfrac{\kappa}{1 + i\tau\omega}} = 1 - \frac{\dfrac{\kappa}{1 + \kappa}}{1 + i\dfrac{\tau}{1 + \kappa}\omega}. \tag{14}$$

This result is strictly equivalent to the approximation of Shapley (1971), who obtained it as a limiting case of a more elaborate treatment, and is closely related to the model of Stevens (1964).

We next turn our attention to $T_L(\omega)$, the transfer function for the lateral inhibitory transduction from impulse rate (in the population of inhibiting ommatidia) to inhibitory post-synaptic potential (in the test ommatidium). This transfer function, like T_s, cannot be measured directly, but it can be determined by two indirect methods, both of which rely on antidromic stimulation of neighboring ommatidia as a source of inhibition on the test ommatidium (Knight et al, 1970). Transfer functions can be measured for the voltage-to-impulse rate transduction in the test ommatidium by passing current through an intracellular microelectrode, and then for the transduction from the (antidromic) impulse rate in the inhibiting units to the reduction of impulse rate in the test ommatidium. The quotient of these two transfer functions yields the transfer function $T_L(\omega)$. Alternatively, one can hyperpolarize the cell to prevent it from firing impulses, and measure the responses of the intracellular potential to antidromic stimulation of neighboring ommatidia, either to brief bursts or to impulse trains with sinusoidally modulated impulse rate. In such hyperpolarized cells, the impulse response to a short burst of antidromic impulses in the neighboring units is well predicted by the inverse Fourier transform of the transfer function describing the response of the same cell to inhibition from

sinusoidally modulated antidromic stimulation of neighboring cells. There is satisfactory agreement between the transfer function measured indirectly as a quotient (with the cell operating at its normal resting potential) and the direct transfer function measurement on the same cell, hyperpolarized.

The lateral inhibitory impulse response typically takes a biphasic form, with a small excitatory effect preceding the main inhibitory hyperpolarization (Knight et al., 1970). We may model this wave form as a combination of four exponential decays. Such a model yields the following expression for the lateral inhibitory transduction, $T_L(\omega)$:

$$T_L(\omega) = \frac{1}{1 - C} \cdot \left[\frac{1}{1 + i\tau_1\omega} \cdot \frac{1}{1 + i\tau_2\omega} - \frac{C}{1 + i\tau_3\omega} \right] \cdot \frac{1}{1 + i\tau_4\omega}. \tag{15}$$

Here, τ_1, τ_2, τ_3, and τ_4 are time constants chosen to fit the inhibitory impulse response, and C describes the relative strength of the brief excitatory feature of the impulse response. The transfer function here is normalized to unity at $\omega = 0$. (The strength of lateral inhibition will be reflected in the inhibitory kernel: see below.)

The remaining transfer functions $\tilde{k}(\xi)$ and $\tilde{P}(\xi)$ depend only on spatial frequency. The two-dimensional inhibitory kernel $k(x, y)$ has been studied extensively, generally by making measurements of inhibitory coupling coefficients in the steady state as a function of distance along the retina (Barlow, 1967, 1969; Johnston and Wachtel, 1976). The data may be summarized as a difference of two-dimensional Gaussian distributions:

$$k(x, y) \propto e^{-\left(x^2 + \frac{y^2}{\eta^2}\right)/a^2} - D \cdot e^{-\left(x^2 + \frac{y^2}{\zeta^2}\right)/b^2}. \tag{16}$$

Here, the main inhibitory feature has a Gaussian distribution whose width is determined by the parameter a, with iso-inhibitory contours whose shape is governed by the parameter η. Barlow's data suggested a small "crater" in the inhibitory kernel, which is similarly described by the second term in Eq. 16. In our one-dimensional situation, we may replace this formula with a simpler form:

$$k(x) = N \cdot \left[Ae^{-x^2/a^2} - Be^{-x^2/b^2} \right], \tag{17}$$

where N is a normalization constant, and the coefficients A and B describe the relative strength of the crater (see Appendix). We may fix the constant N by stipulating that

$$\int_{-\infty}^{\infty} k(x)dx = \mathbf{K}. \tag{18}$$

In the case where the stimulus illuminates the entire vertical extent of the eye, $\mathbf{K}$ is equal to the total inhibition exerted by the entire eye on any one ommatidium. If the stimulus does not cover the entire eye, $\mathbf{K}$ is the total inhibitory strength of the portion of the eye which is illuminated. From Eqs. 17 and 18 we have

$$\mathbf{K} = N \cdot (Aa\sqrt{\pi} - Bb\sqrt{\pi}), \tag{19}$$

or

$$k(x) = \frac{\mathbf{K}}{(Aa - Bb)\sqrt{\pi}} (Ae^{-x^2/a^2} - Be^{-x^2/b^2}). \tag{20}$$

Taking the Fourier transform of Eq. 20 yields the effective one-dimensional transfer function $\tilde{k}(\xi)$:

$$\tilde{k}(\xi) = \int k(x)e^{-i\xi x}dx = \frac{\mathbf{K}}{(Aa - Bb)} (Aae^{-\xi^2a^2/4} - Bbe^{-\xi^2b^2/4}). \tag{21}$$

We note that $\tilde{k}(0) = \mathbf{K}$, as required by Eq. 18.

The point-spread function $P(x)$ describes the distribution on the retina of the image of a "point" stimulus (here, a vertical line). For convenience, we model this function as a normalized Gaussian distribution. This model yields the transfer function

$$\tilde{P}(\xi) = \int_{\infty}^{\infty} P(x)e^{-i\xi x}dx = e^{-\xi^2s^2/4}, \tag{22}$$

where s is a parameter describing the width of the point spread function. Specifically, s is the distance from the center of the image of a point light source to the position where the intensity of the image drops to $1/e$ of its intensity at the center.

A summary of the equations of the Hartline-Ratliff model appears in Table I. This description of the dynamics of the *Limulus* lateral eye contains some 20

TABLE I

SUMMARY OF EQUATIONS FOR THE HARTLINE-RATLIFF MODEL FOR THE *Limulus* LATERAL EYE

Description	Equation no.	Equation
Spatiotemporal transfer function	10	$\mathcal{F}(\xi, \omega)=\frac{M\cdot\tilde{P}(\xi)\cdot E(\omega)\cdot G(\omega)}{1+E(\omega)\cdot T_L(\omega)\cdot\tilde{k}(\xi)}$
Generator potential	11	$G(\omega)=e^{-i\omega t_l}\cdot\left(\frac{1}{1+it_d\omega}\right)^{n_d}\cdot\left(\frac{1}{1+it_b\omega}\right)^{n_b}\cdot\left(1-\frac{R}{1+it_a\omega}\right)\cdot\left(\frac{it_a\omega}{1+t_a\omega}\right)^{p}$
Encoder	14	$E(\omega)=\frac{1}{1+\frac{\kappa}{1+i\tau\omega}}=1-\frac{\kappa/(1+\kappa)}{1+i\frac{\tau}{1+\kappa}\omega}$
Lateral inhibition	15	$T_L(\omega)=\frac{1}{1-C}\cdot\left[\frac{1}{1+i\tau_1\omega}\cdot\frac{1}{1+i\tau_2\omega}-\frac{C}{1+i\tau_3\omega}\right]\cdot\frac{1}{1+i\tau_4\omega}$
Two-dimensional inhibitory kernel	16	$k(x, y)\propto e^{-\left(x^2+\frac{y^2}{\eta^2}\right)/a^2}-D\cdot e^{-\left(x^2+\frac{y^2}{\zeta^2}\right)/b^2}$
One-dimensional inhibitory kernel	20	$k(x)=\frac{\mathbf{K}}{(Aa-Bb)\sqrt{\pi}}\cdot\left(Ae^{-x^2/a^2}-Be^{-x^2/b^2}\right)$
Fourier transform of inhibitory kernel	21	$\tilde{k}(\xi)=\frac{\mathbf{K}}{(Aa-Bb)}\cdot\left(Aae^{-\xi^2a^2/4}-Bbe^{-\xi^2b^2/4}\right)$
Point-spread	22	$\tilde{P}(\xi)=e^{-\xi^2s^2/4}$

nominal parameters. These are constrained, not only to model the overall spatiotemporal transfer function, but also to model each component transduction so as to agree, within reasonable limits, with direct measurements of the corresponding physiological process. For comparison, it may be noted that the empirical spatiotemporal transfer functions, with which the model calculations are to be compared, are obtained by interpolation from 128 independent measurements (amplitude and phase at 64 spatiotemporal frequency pairs).

RESULTS

The results of a typical analysis experiment are shown in Fig. 3. We note the following features: the transfer function shows a marked attenuation of the response to flickering light at very high spatial frequency. Careful inspection of the data indicates that this high frequency cutoff affects the response equally at

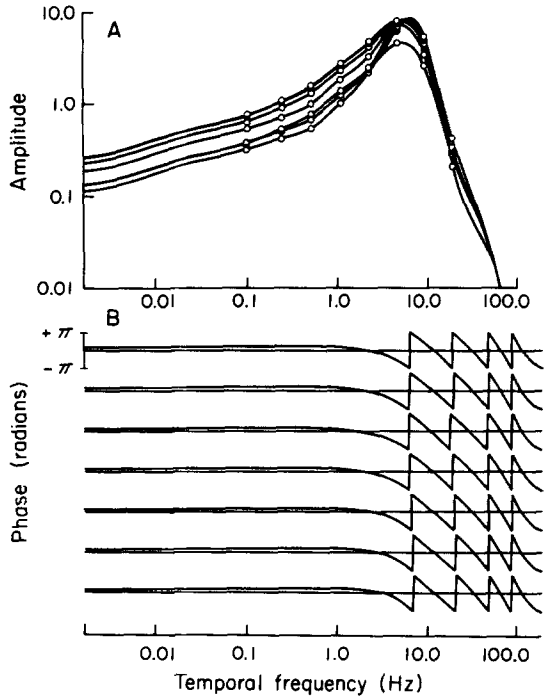

FIGURE 3. Spatiotemporal transfer function for the *Limulus* lateral eye. Bode plots (log amplitude vs. log frequency; phase vs. log frequency) of measured response at seven spatial frequencies (0.1, 1, 2, 4, 8, 16, and 32 cycles/eye width). (A) The amplitude curves are superimposed on one set of axes for comparison (at the peak, near 6 Hz, the amplitudes decrease monotonically with increasing spatial frequency). Data points indicated (O) are direct measurements; the remainder of the curves are interpolated and extrapolated as described in the previous paper (Brodie et al., 1978). Small undulations of the amplitude curves at low frequency are an artifact of the extrapolation procedure. (B) Phase curves are shown on separate axes, modulo 2π; they are extrapolated at the same frequencies as the amplitudes, above. Spatial frequencies increase from bottom to top.

all temporal frequencies; the amplitude is diminished with little change in phase. The behavior at low spatial frequency is more complex, and depends on temporal frequency. At low temporal frequencies, the response to flicker is diminished at low spatial frequency. Conversely, at intermediate temporal frequency, the response to flicker at low spatial frequency is enhanced, as compared to the response at intermediate spatial frequency. At high temporal frequency, there is little dependence on spatial frequency in the low-to-moderate range. The net result is an effective narrowing at low spatial frequency of the "tuning" of the transfer function to a band of intermediate temporal frequency (Ratliff et al., 1967; Ratliff et al., 1969). The general features of the dependence on temporal frequency are a sharp cutoff at high frequency and a broader attenuation of the response to low frequency flicker. Under our conditions, the peak response is at approximately 6 Hz. This is somewhat higher than has been reported previously (Knight et al., 1970), and reflects the elevated temperature of our preparation (Brodie, 1978).

These features may be interpreted as follows: The cutoff at high spatial frequency, which affects all temporal frequencies equally, is presumably due to the degradation of the sinusoidal grating stimulus by the point-spread characteristic of the system optics. At such high spatial frequencies, lateral inhibition is canceled out (see below); thus, the only effect of the optical system is to average the sine-wave grating stimulus so as to reduce its effective contrast at the test ommatidium, reducing the response amplitude equally at all temporal frequencies. The tuning of the frequency response at lower spatial frequencies is presumed to be a consequence of lateral inhibition. The nature of the transition from attenuation (at low temporal frequencies) to enhancement (at intermediate temporal frequencies) to little effect (at high temporal frequencies) is a function of the temporal properties of the lateral inhibitory transduction, T_L. The lateral inhibition increasingly lags in phase with increasing temporal frequency, until, at ~6 Hz, the phase lags by one-half cycle, and the inhibition appears as excitation (Ratliff et al., 1970). The general high temporal frequency cutoff and low frequency attenuation reflect the temporal structure of the generator potential transduction G. The low frequency structure is the result of the "adaptation" process, whereas the high frequency structure depends mainly on the "bump shape."

DATA ANALYSIS AND PARAMETER DETERMINATION

Point-Spread

We now describe a quantitative treatment of some of these features of the spatiotemporal transfer function, in terms of the parameters of the Hartline-Ratliff model. We begin with the attenuation at high spatial frequency. In this regime, the stimulus grating oscillates several times over distances in which the inhibitory kernel presumably varies only slightly. As a result of the linearity of the system, this results in effective cancellation of the time-varying component of the inhibitory action of the retina on the test ommatidium. We therefore may ascribe any dependence of the transfer function on spatial frequency in this regime to the effect of the point-spread transfer function, $\tilde{P}(\xi)$. Since this

function enters the full spatiotemporal transfer function only as a real multiplicative factor, we expect this effect to operate equally at all temporal frequencies, and to produce no phase shift. Hence, for ξ large, Eq. 10 reduces to the simpler approximate form

$$\mathcal{F}(\xi, \omega) = M \cdot \tilde{P}(\xi) \cdot E(\omega) G(\omega), \qquad (\xi \text{ large}). \tag{23}$$

Thus (at high spatial frequencies) for fixed temporal frequency, the transfer function is directly proportional to the point-spread function $\tilde{P}(\xi)$. Accordingly, we may determine the point-spread parameter s in Eq. 22 by plotting, for any fixed temporal frequency ω, the quantity $\log |\mathcal{F}(\xi, \omega)|$ vs. ξ^2; the slope of this line is proportional to s^2. The internal consistency of this determination may be assessed by comparing the s-parameter values obtained from data at several different temporal frequencies from the same preparation. Such an analysis of the high spatial frequency cutoff is shown in Fig. 4. For the preparation of Fig.

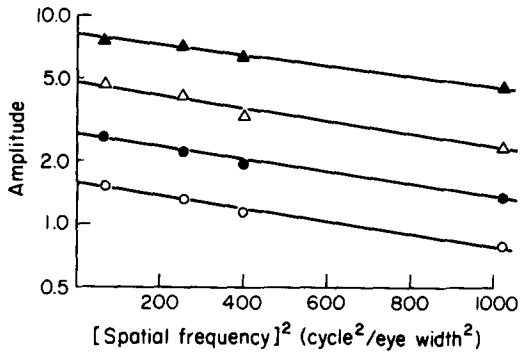

FIGURE 4. Estimation of the point-spread parameter s. For each fixed temporal frequency ω, $\log |\mathcal{F}(\xi, \omega)|$ is plotted vs. ξ^2, the square of the spatial frequency. At high spatial frequency, slope of this locus is $s^2/4$ (see text). Data from the preparation of Fig. 3. Temporal frequencies were 0.5 Hz (○), 1.03 Hz (●), 2.1 Hz (△), and 4.23 Hz (▲). Values for the parameter s were 0.0085, 0.0085, 0.0085, and 0.0078 eye widths, respectively (mean 0.0083 eye widths).

3, we obtain the point-spread parameter value $s = 0.0083$ eye widths. In general, the oberved, point-spread parameter values are comparable to the radius of a *Limulus* ommatidium (0.0125 eye widths), and are thus in good agreement with the estimate of the effective optical point-spread obtained in the preceding article by direct inspection of the crystalline cones (Brodie et al., 1978).

Lateral Inhibitory Kernel

According to our model, the remainder of the dependence of the spatiotemporal transfer function on spatial frequency is due to the structure of the inhibitory kernel $k(x)$, as reflected in its Fourier transform $\tilde{k}(\xi)$. In order to determine this function from the experimental data, we have found it expedient to work with plots of the locus, on the complex plane, of $1/\mathcal{F}(\xi, \omega)$ as a function

of spatial frequency (ξ), with temporal frequency (ω) fixed. From Eq. 10 we have

$$\frac{1}{\mathcal{F}(\xi, \omega)} = \left[\frac{1}{\tilde{P}(\xi)} \cdot \frac{1}{E(\omega)G(\omega)} + \frac{\tilde{k}(\xi)}{\tilde{P}(\xi)} \cdot \frac{T_L(\omega)}{G(\omega)}\right] \cdot \frac{1}{M}. \tag{24}$$

This function has an extremely convenient form: it is a sum of two terms, each of which is a (complex) function of temporal frequency multiplied by a real function of spatial frequency. For fixed ω, we may regard the complex numbers $1/E(\omega)G(\omega)$ and $T_L(\omega)/G(\omega)$ as fixed vectors in the complex plane. As ξ varies, this reciprocal locus traces out a weighted sum of these two vectors (Fig. 5). Interpretation of these loci is considerably simplified by the fact that the spatial transfer functions $\tilde{P}(\xi)$ and $\tilde{k}(\xi)$ vary strongly with ξ in different regions of spatial frequency. Thus, for low and intermediate values of ξ, where $\tilde{k}$ is of

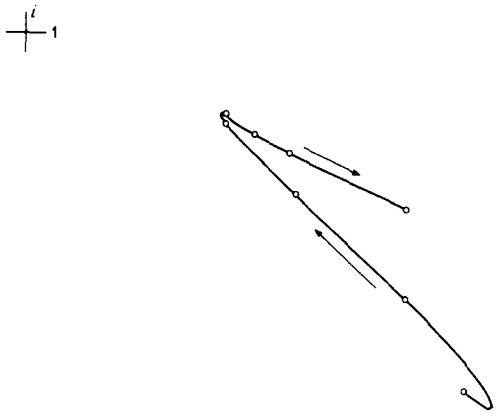

FIGURE 5. Reciprocal locus. The locus of the reciprocal of the measured spatiotemporal transfer function is plotted on the complex plane as a function of spatial frequency, with temporal frequency held fixed. Data from Fig. 3, with temporal frequency held at 1.03 Hz. Points at which measurements were made are indicated (O). The arrows indicate the direction of increasing spatial frequency along the locus. The loop at the low frequency end of the locus is an artifact of the spline interpolation procedure used to generate the curve.

interest, the function $\tilde{P}(\xi)$ is nearly constant; conversely, at high spatial frequency, where $\tilde{P}$ shows structure of interest, $\tilde{k}$ has fallen essentially to zero. Thus, the reciprocal loci have a basic V-shaped form, first moving toward the origin along a vector parallel to $T_L(\omega)/G(\omega)$, then moving away from the origin along the vector $1/E(\omega)\cdot G(\omega)$. This separation of the scales of the functions $\tilde{P}(\xi)$ and $\tilde{k}(\xi)$ corresponds to the fact that the point-spread function $P(x)$ is considerably narrower than the narrowest feature of the inhibitory kernel $k(x)$.

We may further isolate the role of the inhibitory kernel by multiplying Eq. 24 by the point-spread transfer function $\tilde{P}(\xi)$:

$$\frac{\tilde{P}(\xi)}{\mathcal{F}(\xi, \omega)} = \left[\frac{1}{E(\omega)G(\omega)} + \tilde{k}(\xi) \cdot \frac{T_L(\omega)}{G(\omega)}\right] \cdot \frac{1}{M}. \tag{25}$$

The quantity on the left of this equation may be thought of as the reciprocal of the spatiotemporal transfer function, "corrected" for the effect of the point-spread function. If we now hold ω fixed and plot on the complex plane the locus of Eq. 25 as a function of ξ, we obtain a corrected reciprocal locus, which traverses a line parallel to the vector $T_L(\omega)/G(\omega)$, according to the function $\tilde{k}(\xi)$ (Fig. 6). We may fix a reference point on this locus by considering the limit of high spatial frequency. In this limit, $\tilde{k}(\xi)$ approaches zero, as described above, and we have the asymptotic result:

$$\frac{\tilde{P}(\xi)}{\mathcal{F}(\xi, \omega)} = \frac{1}{E(\omega)G(\omega)} \cdot \frac{1}{M}, \qquad (\xi \text{ large}). \tag{26}$$

Equivalently, we may fix this reference point as the intersection of the high frequency asymptote of the reciprocal locus (Eq. 24) with the low frequency arm

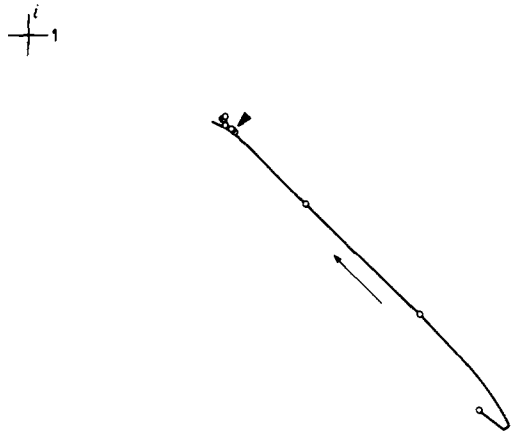

FIGURE 6. Corrected reciprocal locus. The locus of the product of the reciprocal of the measured transfer function (data of Fig. 3, 1.03 Hz) and the estimated point-spread transfer function (Eq. 22, s-parameter determined from data of Fig. 4) is plotted as a function of spatial frequency, with temporal frequency held fixed. Points at which measurements were made are indicated (○); the point of reference for the measurement of the inhibitory kernel transform $\tilde{k}(\xi)$ is indicated by the large arrowhead. Arrow indicates direction of increasing spatial frequency.

of the locus. This point presumably describes the phase of the system's response in the complete absence of lateral inhibition (Fig. 6).

Once this reference point is located on the corrected reciprocal locus, we may then directly measure the signed distances of the points $\tilde{P}(\xi)/\mathcal{F}(\xi, \omega)$ of the locus from this reference point. These distances, as a function of ξ, are proportional to $\tilde{k}(\xi)$, the Fourier transform of the inhibitory kernel.

Typical results of this procedure are shown in Fig. 7. The measured values for $\tilde{k}(\xi)$ have been interpolated linearly. Though the data are somewhat noisy at high spatial frequency, where the attenuation of the response reduces the signal-to-noise ratio, the basic form of the function is clear. The transform $\tilde{k}$ falls rapidly from its initial value, overshoots the reference point where $\tilde{k} = 0$,

and, at high spatial frequency, slowly returns to zero from below. This overshoot corresponds to the slight offset of the vertex of the V-shaped reciprocal locus to the opposite side of the high frequency asymptote from the low frequency end of the locus (Fig. 5). This overshoot may be considered as evidence, in the spatial frequency domain, for a small "crater" in the inhibitory kernel $k(x)$.[3] In essence, at intermediate spatial frequency, the broad inhibitory portion of the kernel is cancelled by the oscillation of the grating stimulus, but the narrower, oppositely signed component can still resolve the grating, and results in a reversal in the sign of the time-dependent inhibitory effect. This qualitative indication of the presence of a crater in the inhibitory kernel represents an important advantage of sinusoidal gratings over single bars of varying width as a test stimulus for the analysis of the spatial organization of such a system. The inhibitory kernel $k(x)$ may be obtained from these data by taking the inverse Fourier transform of the measured function $\tilde{k}(\xi)$ (Fig. 7). In both the space and spatial frequency domains, there is essential agreement between the inhibitory kernel measurements at the different temporal frequencies. This verifies the internal consistency of these measurements, and the applicability of the Hartline-Ratliff model (Eq. 10).

The inhibitory kernel data at the various temporal frequencies were averaged together (Fig. 8). This averaged kernel was then fitted by eye with a difference of two Gaussian distributions, according to Eq. 17. The parameters of this model kernel specify the geometry of the inhibitory field. For the preparation of Fig. 3, we obtained the following values: $A = 2.06, a = 0.17$ eye widths; $B = 1.2, b = 0.025$ eye widths. Similar data obtained in this way from several preparations all strongly imply the existence of a small crater in the inhibitory kernel.

This fitting procedure was also used for one experiment in which the usual stimulus was rotated 90°, so as to produce a vertical band of light whose intensity varied sinusoidally as a function of y, the vertical coordinate. The inhibitory kernel in the vertical direction was found to be similar to that in the horizontal direction, with a large Gaussian inhibitory lobe, and a small crater surrounding the test ommatidium. (Parameters $A = 3.7, a = 0.09$ eye widths, $B = 0.9, b = 0.02$ eye widths.)

Total Inhibitory Strength

The total inhibitory strength **K** is best determined at very low temporal frequencies, where there is no significant phase lag between excitation and inhibition, and where we may treat the response amplitude as a simple scalar sum of excitation and inhibition. As ω approaches zero, we obtain the following limiting form for Eq. 10:

$$\mathcal{F}(\xi, \omega) = \frac{M \cdot \tilde{P}(\xi) \cdot (1 - R) \cdot (i\omega)^p \cdot \left(\frac{1}{1 + \kappa}\right)}{1 + \tilde{k}(\xi)/(1 + \kappa)}, \qquad (\omega \text{ small}). \tag{27}$$

[3] Such an overshoot can also correspond to a slight flattening of the peak of the inhibitory kernel, rather than an actual crater, depending on the strength of the overshoot. In general, the overshoot corresponds to a crater whenever $\int_0^\infty \xi^2 k(\xi) d\xi < 0$.

Because the scales of $\tilde{P}(\xi)$ and $\tilde{k}(\xi)$ are well separated (see above), we may ignore the point-spread function $\tilde{P}(\xi)$ for low and moderate spatial frequencies, where $\tilde{P}(\xi) \cong 1$. With this approximation, we may attribute all of the dependence of the response amplitude in this regime of spatial frequency to the effect of lateral inhibition. The total extent of this dependence directly reflects the total inhibitory strength **K** as follows: we define ξ_0 as that spatial frequency at which the inhibitory transfer function $\tilde{k}(\xi)$ first crosses the ξ-axis (Fig. 9). At this spatial frequency, the effect of the crater in the inhibitory kernel exactly cancels the

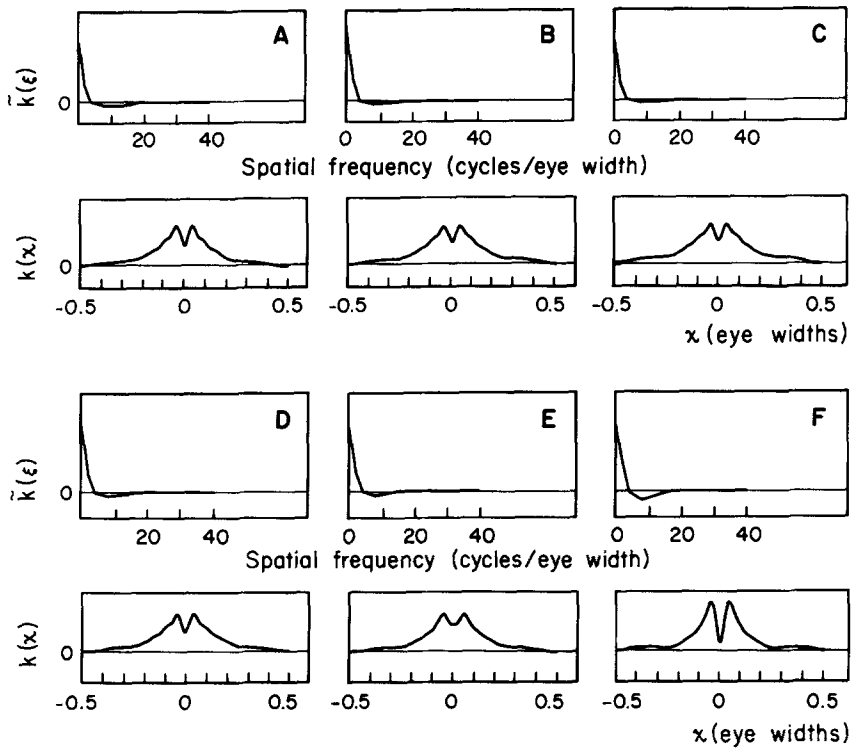

FIGURE 7. Inhibitory kernel measurements. For each of six temporal frequencies, the inhibitory transfer function $\tilde{k}(\xi)$ and the corresponding inhibitory kernel $k(x)$ are shown. Inhibitory transfer functions obtained from measurements of corrected reciprocal loci, as in Fig. 6; each inhibitory kernel is the inverse Fourier transform of the corresponding inhibitory transfer function. Data from Fig. 3; temporal frequencies are (A) 0.1 Hz, (B) 0.23 Hz, (C) 0.5 Hz, (D) 1.03 Hz, (E) 2.1 Hz, (F) 4.23 Hz.

effect of the main inhibitory part of the kernel, and the test ommatidium sees no time-dependent inhibition: thus,

$$\mathcal{F}(\xi_0, \omega) = M \cdot (1 - R) \cdot (i\omega)^p \cdot \left(\frac{1}{1 + \kappa}\right), \qquad (\omega \text{ small}). \tag{28}$$

On the other hand, we have $\tilde{k}(0) = \mathbf{K}$, whence

$$\mathcal{F}(0, \omega) = \frac{M \cdot (1 - R)(i\omega)^p \left(\frac{1}{1 + \kappa}\right)}{1 + \mathbf{K}/(1 + \kappa)}, \qquad (\omega \text{ small}). \tag{29}$$

We thus obtain the following expression for the (observable) quotient $Q_0 = \mathcal{F}(\xi_0, \omega)/\mathcal{F}(0, \omega)$:

$$Q_0 = \frac{M(1 - R)(i\omega)^p \left(\frac{1}{1 + \kappa}\right)}{M(1 - R)(i\omega)^p \left(\frac{1}{1 + \kappa}\right) \Big/ \left(1 + \frac{\mathbf{K}}{1 + \kappa}\right)} = 1 + \frac{\mathbf{K}}{1 + \kappa}, \tag{30}$$

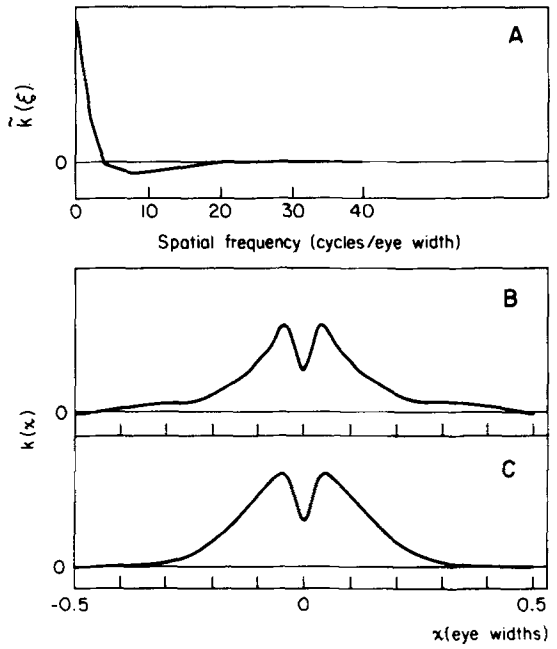

FIGURE 8. (A) Averaged inhibitory transfer function, from data of Figure 7. (B) Averaged inhibitory kernel, obtained as inverse Fourier transform of (A). (C) Model inhibitory kernel (Eq. 17), fitted by eye to measured kernel of (B). Parameters are $A = 2.2, a = 0.17$ eye widths, $B = 1.2, b = 0.025$ eye widths.

or

$$\frac{\mathbf{K}}{1 + \kappa} = Q_0 - 1. \tag{31}$$

Alternatively, we may define ξ_1 as that spatial frequency at which the inhibitory transfer function $\tilde{k}(\xi)$ takes on its most negative value (Fig. 9). Near this spatial frequency (for low temporal frequency), the effect of the lateral ("inhibitory")

interaction is to enhance the response of the test ommatidium; at $\xi = \xi_1$, the response is maximal. If we set $\tilde{k}(\xi_1) = -\theta\tilde{k}(0) = -\theta \cdot \mathbf{K}$, we have

$$\mathcal{F}(\xi_1, \omega) = \frac{M(1 - R) \cdot (i\omega)^p \cdot \left(\frac{1}{1 + \kappa}\right)}{1 - \frac{\theta \mathbf{K}}{1 + \kappa}}. \tag{32}$$

We may thus form the (observable) quotient $Q_1 = \mathcal{F}(\xi_1, \omega)/\mathcal{F}(0, \omega)$:

$$Q_1 = \frac{M(1 - R)(i\omega)^p \cdot \left(\frac{1}{1 + \kappa}\right) \Big/ \left(1 - \frac{\theta \mathbf{K}}{1 + \kappa}\right)}{M(1 - R)(i\omega)^p \cdot \left(\frac{1}{1 + \kappa}\right) \Big/ \left(1 + \frac{\mathbf{K}}{1 + \kappa}\right)} = \frac{1 + \frac{\mathbf{K}}{1 + \kappa}}{1 - \frac{\theta \mathbf{K}}{1 + \kappa}}, \tag{33}$$

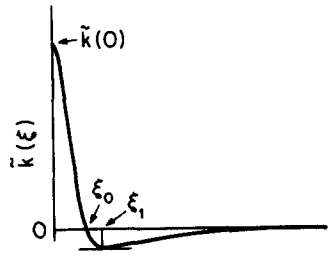

FIGURE 9. Determination of total inhibitory strength. Characteristic spatial frequencies ξ_0 and ξ_1 are defined from the measured spatial inhibitory transfer function $\tilde{k}(\xi)$ as shown. The parameter θ is determined as the ratio $-\tilde{k}(\xi_1)/\tilde{k}(0)$. For the data of Fig. 3, this procedure produced quotients $Q_0 = 2.545$, $Q_1 = 2.63$ ($\theta = 0.069$), yielding estimates of $\mathbf{K}/(1 + \kappa) = 1.545$ and 1.380, respectively (see text).

or

$$\frac{\mathbf{K}}{1 + \kappa} = \frac{Q_1 - 1}{1 + \theta \cdot Q_1}. \tag{34}$$

These two estimates depend on observation of somewhat different features of the low frequency transfer function, and provide a check on each other (Fig. 9). For the preparation of Fig. 3, we obtained the values $Q_0 = 2.545$, $Q_1 = 2.63$ ($\theta = 0.069$), yielding estimates of $\mathbf{K}/(1 + \kappa) = 1.545$ and 1.380, respectively. (Our model transfer function (Fig. 12) was calculated with $\mathbf{K}/(1 + \kappa) = 1.3$, which fit the data slightly better.) The occurrence of the quotient $\mathbf{K}/(1 + \kappa)$ on the left of Eq. 31 and 34 reflects the fact that the lateral inhibitory transduction follows the encoder transduction, and cannot be studied in isolation by our methods.

The transfer functions which remain to be determined are those that depend only on temporal frequency: $E(\omega)$, $G(\omega)$, and $T_L(\omega)$. These functions determine the directions and lengths of the "arms" of the reciprocal loci at the different

temporal frequencies (Fig. 10), but because they occur as products or quotients in Eq. 25 it is difficult to extract the model parameters for these functions directly from measurements of these loci, as was done for the spatial transfer functions. Instead, we have found it convenient to adjust these parameters so as to match the Bode plots of the complete spatiotemporal transfer function (Fig. 11); the reciprocal loci calculated for the model transfer function then serve to check the accuracy of the model. Below, we discuss the extent to which the individual parameters can be associated with specific features of the measured transfer function.

Generator Potential

We begin with the generator potential transfer function $G(\omega)$ (Eq. 11). The most prominent feature of the generator potential transfer function is the severe

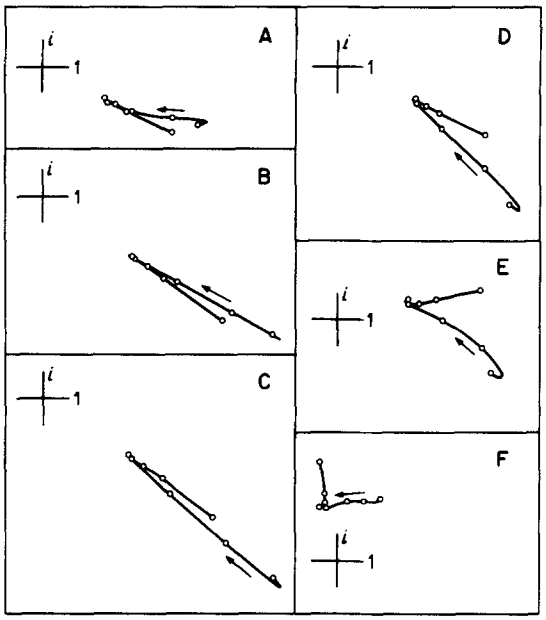

FIGURE 10. Reciprocal loci, as in Fig. 5, are plotted for six temporal frequencies: (A) 0.1 Hz, (B) 0.23 Hz, (C) 0.5 Hz, (D) 1.03 Hz, (E) 2.1 Hz, and (F) 4.23 Hz. The loci have been magnified by factors of 1, 2, 3, 4, 6, and 8, respectively. Arrows indicate direction of increasing spatial frequency.

cutoff at high frequencies. This is a consequence of the two factors of the form $\left(\frac{1}{1 + i\omega t}\right)^n$. In general, such a factor produces a severe attenuation at frequencies exceeding $1/t$. Thus, the time constants in these factors can be estimated by noting the frequency at which the high-frequency cutoff begins. In practice, the two factors of this form are not separable in terms of their effect on the overall transfer function. However, they have been independently measured in excised preparations by Wong, who measured the intracellular voltage directly by

means of intracellular microelectrodes (Wong, 1977).[2] Such measurements provide starting points for estimates of the parameters for our data. For example, Wong's values for t_d, the time constant for dispersion of bump latencies, were approximately one-half of his values for t_b, the time constant for

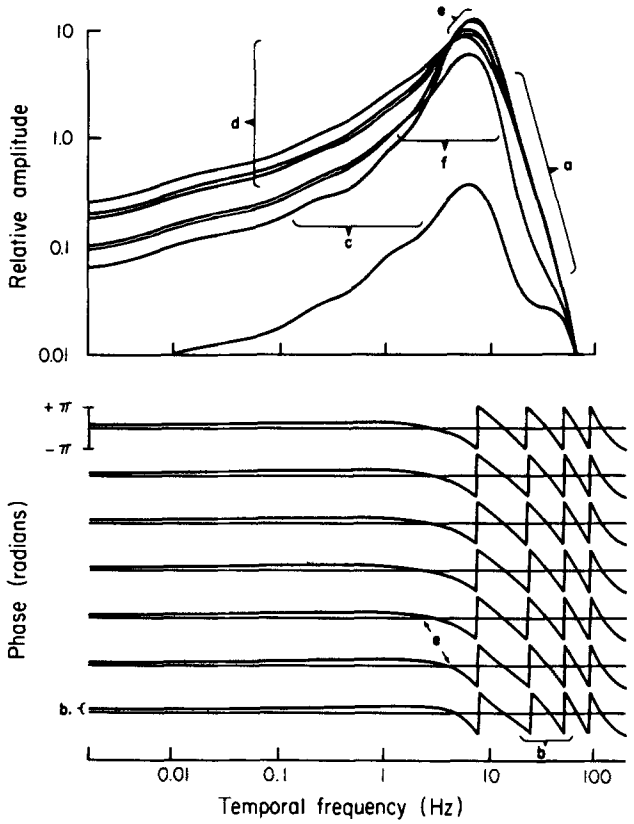

FIGURE 11. Estimation of temporal transfer function parameters. The features indicated depend most strongly on particular transfer function parameters, as shown, and were used to fit these parameters, as discussed in the text. (*a*) High-frequency cut-off determines generator potential time constants t_d and t_b. (*b*) Steepness of phase lag determines exponents n_d and n_b; low-frequency phase lead determines time-constant t_l. (*c*) Frequency range of adaptation effect determines time constant t_a. (*d*) Magnitude of adaptation effect determines adaptation coefficient R. (*e*) Low spatial frequency tuning amplitude peak and phase dependence fitted by strength κ and time constant τ for encoder transfer function $E(\omega)$. (*f*) Lateral inhibitory transfer function $T_L(\omega)$ adjusted to fit fine structure of spatial dependence at intermediate temporal frequencies. Data from Brodie et al. (1978), Fig. 4 A, B.

the bump shape; we have preserved this relationship in our choice of parameters to describe the preparation of Fig. 3: $t_d = 0.0091$ s, $t_b = 0.019$ s.

The exponents n_d and n_b control the steepness of the high-frequency amplitude cutoff (as opposed to the frequency at which it occurs), and also the

rate of increase of the high-frequency phase lag of the generator potential transfer function with increasing frequency. For our data, the phase effect proved very dramatic, and unambiguously determined our choice of $n_d + n_b = 8$. This choice of exponents is consistent with Wong's more direct measurements. The time constant t_l, the mean latency of the voltage bumps, produces a small adjustment in the phase of the response, with no effect on amplitude. For the data of Fig. 3, we used $t_l = 0.023$ s.

Adaptation Parameters

We consider next those parameters of the generator potential transfer function which describe the adaptation process. For the exponent in the factor

$$[it_a\omega/(1 + it_a\omega)]^p,$$

we chose the value $p = 0.25$, as suggested by the measurements of low-frequency transfer function data by Biederman-Thorson and Thorson (1971). This choice of exponent is consistent with our measurements below 1 Hz, and, as described in the preceding article, it correctly accounts for the response of the eye to slowly moving stimuli (Brodie et al., 1978). The adaptation time constant t_a determines the frequency above which adaptation ceases to significantly affect the response of the eye; it may be estimated from the position (relative to the frequency axis) of the increasing portion of the amplitude data (see Fig. 11). For the data of Fig. 3, the value $t_a = 0.020$ s was chosen.

There remains to be determined the parameter R in the factor

$$(1 - R/[1 + it_a\omega]),$$

which governs the magnitude of the adaptation effect. In the absence of lateral inhibition, the effect of this factor cannot be formally distinguished from the effect of self-inhibition, which is described by a factor of similar form. On the other hand, unlike light adaptation, self-inhibition modifies the effect of lateral inhibition. This allows the independent determination of the parameters of self-inhibition (see below). Once these are estimated, the parameter R may then be adjusted to account for the residual attenuation of the response at low frequencies. (The ratio of the response at low frequencies to that at intermediate frequencies is proportional to $1 - R$.) For the preparation of Fig. 3, this procedure resulted in the value $R = 0.89$.

Lateral Inhibition

The lateral inhibition transfer function $T_L(\omega)$ is described by four time constants and the ratio of the initial excitatory component to the main inhibitory component (Eq. 15). This transfer function controls the transition from attenuation to enhancement of the response to low spatial frequency gratings as temporal frequency increases; it also controls the high-frequency cutoff of lateral inhibition, which sets in at somewhat lower frequencies than the cutoff of the generator potential. The calculated transfer function is most sensitive to these parameters in the region of the "inversion" of the sign of the lateral "inhibitory" interaction (see Fig. 11), though it is difficult to systematically describe the effects of the individual time constants. For the data of Fig. 3, the best fit was obtained with the magnitude C of the excitatory component set equal to zero; the corresponding time constant τ_3 becomes undefined. The

other time constants, which then become formally equivalent, were given values of 0.0415, 0.0415, and 0.010 s.

Self-Inhibition

The effects of self-inhibition are contained in the transfer function of the encoder mechanism, $E(\omega)$. This transfer function occurs twice in the Hartline-Ratliff model (Eq. 10): in the numerator, where it describes a high-pass characteristic of the excitatory process, and in the denominator, where it represents a similar feature of the lateral inhibitory process. As mentioned above, it is difficult to separate the effect of self-inhibition on the excitatory process from that of light adaptation, though direct measurements of self-inhibition suggest it is a much slower process. We therefore relied mostly on the modulation of lateral inhibiton by self-inhibition to determine the self-inhibitory parameters.

It may be recalled that the ratio $\mathbf{K}/(1 + \kappa)$ was directly determined from the transfer function data at low frequency. With this parameter regarded as fixed, the effect of self-inhibition is to adjust the magnitude of the "inhibitory" tuning effect seen in the intermediate temporal frequency range at low spatial frequencies.[4] Thus, the size of this tuning peak effectively fixes the strength of self-inhibition. For the data of Fig. 3, the value $\kappa = 1.0$ was obtained. The time constant τ was then selected to best fit the overall width of the transfer function peaks. For the data of Fig. 3, the value $\tau = 0.125$ s was chosen. This confirms our assumptions that self-inhibition is considerably slower than light adaptation ($t_a = 0.020$ s). After the parameters for self-inhibition were estimated, the adaptation parameters were readjusted as described above. No further improvement in the fit of the model was obtained by further iterating the procedure.

Once all these parameters have been estimated, the complete model transfer function can be compared with the data in several ways. A Bode plot of the Hartline-Ratliff transfer function is shown in Fig. 12; it is to be compared directly with Fig. 3. All of the qualitative features discussed above are well modeled, as are most of the quantitative features.[5] The reciprocal loci offer another comparison between the model and the data: Fig. 13 shows the locus for a temporal frequency of 1.03 Hz, and should be compared with Fig. 5. Loci for several temporal frequencies are shown in Fig. 14 (compare with Fig. 10). The reciprocal loci are well modeled over a broad range of temporal frequen-

[4] This may be demonstrated as follows: as above, define ξ_0 such that $k(\xi_0) = 0$, and set

$$Q_0 = \mathcal{F}(\xi_0, 0)/\mathcal{F}(0, 0) = 1 + \frac{\mathbf{K}}{1+\kappa}. \qquad \text{(Eq.30)}$$

We regard Q_0, and hence $\mathbf{K}/(1 + \kappa)$ as known. Define ω_p as the frequency such that $|\mathcal{F}(0, \omega_p)|$ is maximal, and set $W = \mathcal{F}(0, \omega_p)/\mathcal{F}(\xi_0, \omega_p)$. W is very nearly real, and measures the magnitude of the tuning effect. As we may safely assume that $E(\omega_p) \cong 1$, we have $\mathcal{F}(0, \omega_p) = G(\omega_p)/(1 + \mathbf{K}T_L(\omega_p))$, and $\mathcal{F}(\xi_0, \omega_p) = G(\omega_p)$. This yields

$$W = 1/(1 + \mathbf{K}T_L(\omega_p)) = 1/(1 + (1 + \kappa)(Q_0 - 1)T_L(\omega_p)).$$

As Q_0 and T_L have been determined, we now fit W by adjusting κ. (Here, $T_L(\omega_p)$ is a complex number whose phase is typically such that increasing κ actually increases $|W|$.)

[5] A somewhat similar model transfer function, based on nominal parameters for excised *Limulus* eyes, is described by Leung and Freeman (1977).

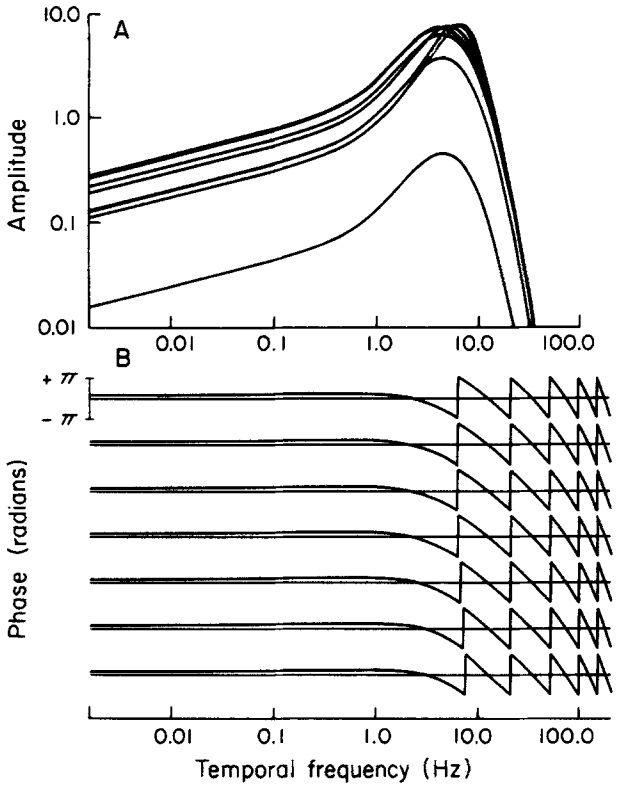

FIGURE 12. Hartline-Ratliff model spatiotemporal transfer function for the *Limulus* lateral eye. Bode plots (as in Fig. 3) of predicted response at seven spatial frequencies. Curves are obtained from the equations given in the text (see Table I), with parameters chosen to fit empirical transfer function of Fig. 3 (see Table II).

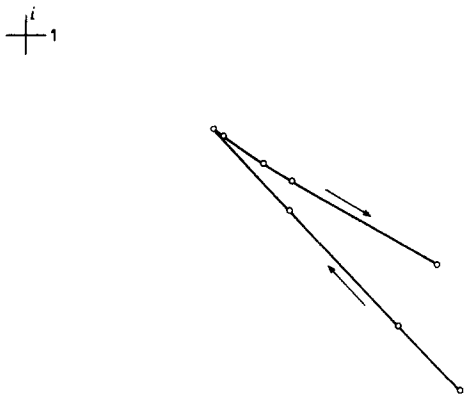

FIGURE 13. Reciprocal locus for temporal frequency of 1.03 Hz, as predicted by Hartline-Ratliff model, with parameters as in Fig. 12. Compare with Fig. 5.

cies. The parameters for the transfer function of Figs. 12, 13, and 14 are summarized in Table II.

An alternative strategy for evaluating the accuracy of the Hartline-Ratliff model is to use the empirical and model transfer functions to produce Fourier syntheses of the response of the eye to a moving stimulus, as described in the preceding article. Such predictions are extremely accurate, and can be relied upon to characterize the eye, even when such moving stimuli were not included in the experimental protocol (Brodie et al., 1978). Predictions for the response to a square-wave stimulus moving at several different velocities are shown in Fig. 15. There is excellent agreement between the predictions derived from the

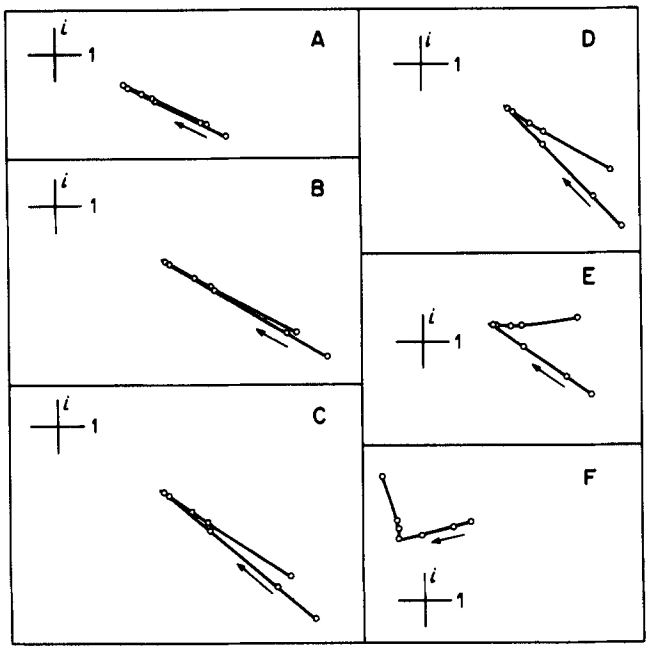

FIGURE 14. Reciprocal loci for six temporal frequencies, as predicted by Hartline-Ratliff model, with parameters as in Fig. 12 (Table II). Compare with Fig. 10. Temporal frequencies are (A) 0.1 Hz, (B) 0.23 Hz, (C) 0.5 Hz, (D) 1.03 Hz, (E) 2.1 Hz, (F) 4.23 Hz. Loci are magnified by relative factors of 1, 2, 3, 4, 6, and 8, respectively.

measured transfer function and the Hartline-Ratliff model. The few small discrepancies are comparable to those typically seen between actual measured responses to moving stimuli and the Fourier synthesis predictions of these responses from measured transfer function data.

A complete linear systems-analysis treatment of the *Limulus* eye is represented in Fig. 16, which allows comparison of measured responses to moving square-wave stimuli with the Fourier synthesis predictions obtained from the empirically measured transfer function (Brodie et al., 1978) and a transfer function calculated from the Hartline-Ratliff model (parameters are given in Table II).

The principal features of these square-wave responses may be readily interpreted in terms of the Hartline-Ratliff model. At low velocities, lateral inhibition precedes the arrival of the step at the test ommatidium, resulting in an anticipatory "Mach band" in the impulse rate, just before the on-transient. Also, at low drift velocities, the on-transient itself is much attenuated. This is due to the predominance of low-frequency components (to which the eye is relatively insensitive) in the low-velocity stimuli. This predominance is further enhanced

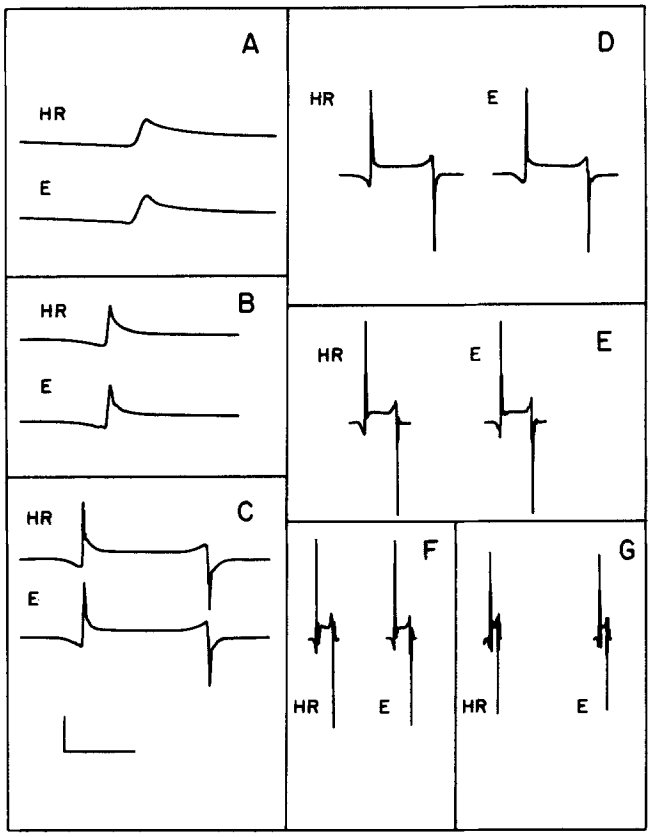

FIGURE 15. Fourier synthesis of the response to a moving square-wave stimulus at several velocities. For each velocity, *E* denotes response calculated from empirically measured transfer function (Fig. 3), and HR denotes response calculated from Hartline-Ratliff model transfer function, with parameters as in Table II (Fig. 12). Drift velocities: (A) 0.01, (B) 0.03, (C) 0.06, (D) 0.12, (E) 0.24, (F) 0.48, (G) 0.96 eye widths/s. Scale marker: horizontal, 10 s; vertical, 10 impulses/s.

by the optical point-spread effect, which filters out the high (spatial) frequency components from the moving stimuli. At higher velocities, the on-transient becomes very pronounced as the stimulus contains greater spectral power at frequencies near the peak of the spatiotemporal transfer function. Due to the

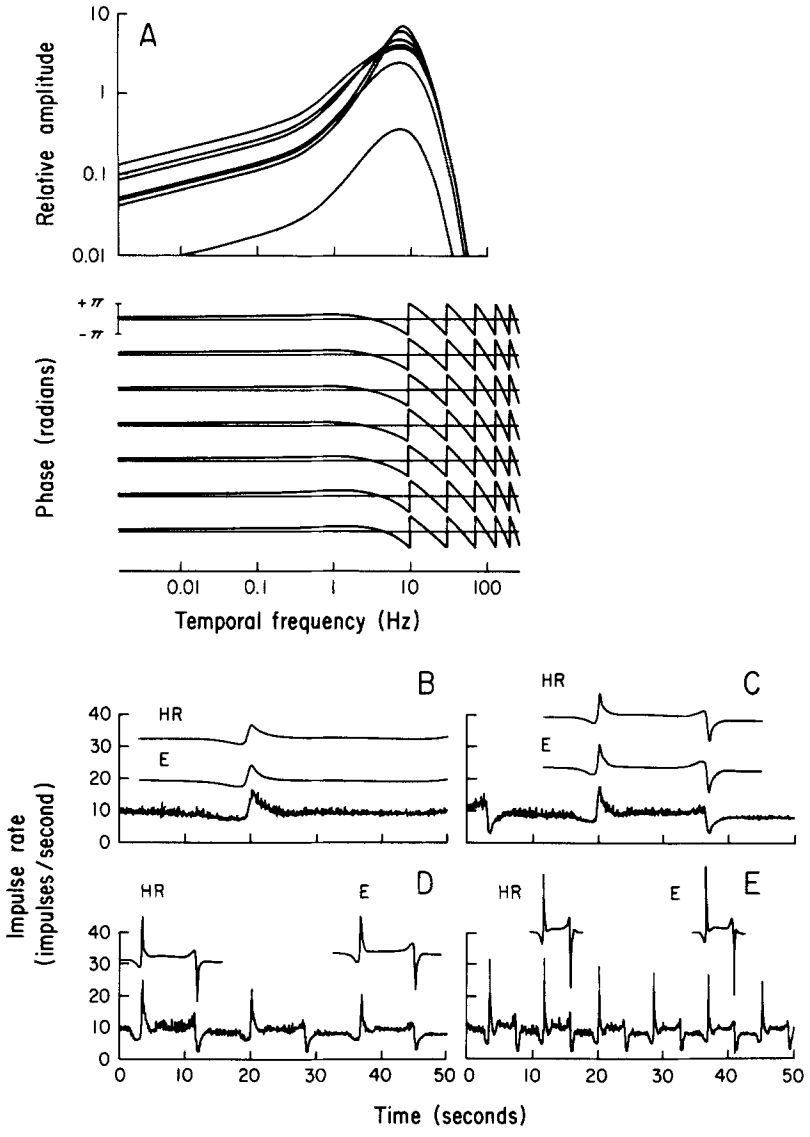

FIGURE 16. Fourier synthesis of the response to moving square-wave stimuli: comparison with measured response. (A) Hartline-Ratliff model spatiotemporal transfer function, with parameters chosen to fit empirical transfer function of Fig. 11 (see Table II). (B–E) Comparison of measured response to moving square wave, response calculated from empirically measured transfer function (E), and response calculated from Hartline-Ratliff model transfer function with parameters as in (A) above (HR). Drift velocities: (B) 0.03, (C) 0.06, (D) 0.12, and (E) 0.24 eye widths/s. Response records from Brodie et al., 1978, Fig. 7.

TABLE II

PARAMETERS FOR THE HARTLINE-RATLIFF MODEL

Parameter	Description	Dimension	Preparation of Fig. 3	Preparation of Fig. 11
M	Normalization constant		*	*
t_l	mean bump latency	s	0.023	0.023
t_d	latency dispersion time constant	s	0.0091	0.0076
n_d	dispersion exponent		4	4
t_b	bump shape time constant	s	0.0019	0.0017
n_b	bump shape exponent		4	4
R	adaptation strength		0.89	0.96
t_a	adaptation time constant	s	0.020	0.013
p	low-frequency adaptation exponent		0.25	0.25
κ	self-inhibitory strength		1.0	0.5
τ	self-inhibitory time constant	s	0.125	0.125
τ_1	lateral inhibitory time constant	s	0.0415	0.033
τ_2	lateral inhibitory time constant	s	0.0415	0.050
τ_3	lateral inhibitory time constant	s	‡	0.033
τ_4	lateral inhibitory time constant	s	0.010	0.017
C	lateral inhibition structure constant		0	0.1
K	total lateral inhibitory strength		2.60	1.60
A	inhibitory strength (relative)		2.06	1.00
a	inhibitory space constant	eye widths	0.17	0.182
B	crater strength (relative)		1.20	1.92
b	crater space constant	eye widths	0.025	0.027
s	point-spread space constant	eye widths	0.0083	0.016

* M is a scale parameter that cannot be directly related to the physiology of the eye on the basis of our measurements. It has been set to different values in the various model calculations, as convenient.

‡ Time constant undefined when C = 0.

nature of a step-transient stimulus, the on-transient of the response remains large even at very great velocities.[6]

DISCUSSION

The data presented above clearly demonstrate the adequacy of the Hartline-Ratliff model to explain the dynamic properties of the *Limulus* lateral eye, at least those properties concerned with its responses to small and moderate changes in light intensity around a mean operating level. Conversely, the success of this analytic program demonstrates the suitability of our analysis

[6] It should be noted that the computations (similar to those of Fig. 15) of Knight (1973 *a*), contain a systematic error in velocity. The velocities given in Fig. 38 there should be multiplied by 2π. Those calculations did not allow for the point-spread effect. The model transfer function used for the calculations was based on parameters for excised eyes at room temperature (Knight et al., 1970). Our heated, intact preparations show a considerably faster response (see Appendix); we calculate that, in our preparations, only steps moving at speeds of at least 2 eye widths/s will produce responses with little or no inhibitory "Mach band" precursor.

stimuli, which consist of sinusoidal gratings in space modulated according to a sum-of-sinusoids signal in time, for the characterization of this sensory transducer.

Although the overall performance of the model is excellent, we are not in a position to assess the goodness-of-fit in quantitative terms, as there is no well-established estimator of the "distance" between two spatiotemporal transfer functions. Nevertheless, we can state that, except as noted below, the parameters given above are "correct" to within a few percent, in the sense that alteration of any individual parameter by more than that amount produces a demonstrably inferior fit of the model transfer function to the data. We have also considered the possibility of trade-offs between certain parameters (such as those of light adaptation and self-inhibition). While such trade-offs do occur, the fits obtained with the parameters given above are in general at least as good as those obtained with alternative choices.

Our characterization of the point-spread phenomenon is simple and reliable. The measurements of the inhibitory kernel are more complex. This determination depends strongly on the phase information at high spatial frequency, in order to determine a reference point for the measurement of $\bar{k}$ from the corrected reciprocal locus. Such phase data are least reliable at these high spatial frequencies, because the point-spread effect substantially attenuates the response to the high-frequency gratings. Nonetheless, at least for data taken below 5 Hz, the consistency of the measurements is very good. (At higher frequencies, there is sufficient noise in the phase data to render impossible measurements of the inhibitory kernel from data at these frequencies.) Our estimates of the size and strength of the main inhibitory lobe of the kernel are strongly confirmed by the Fourier synthesis calculation at low velocity, which is very sensitive to this feature. Although the data consistently indicate, by the characteristic offset of the vertex of the reciprocal locus, the presence of a small crater in the inhibitory kernel, our estimates of its width and strength are somewhat crude (see Appendix).

The bump-shape parameters of the generator potential transfer function are strongly reflected in the high-frequency amplitude and phase data, and are therefore reliably determined, at least to the extent that they are in principle separable from one another. The strength and time constant for light adaptation are also well determined. It is not possible to model the data in such a way that adaptation and self-inhibition have similar time constants, or are combined into a single process.

The parameters for the temporal structure of lateral inhibition are buried rather deeply in the model. In particular, the structure constant describing the strength of the initial excitatory feature has little effect on the computed transfer functions; most of the effective delay of the inhibitory transient is accounted for by the three low-pass filter stages. Nonetheless, even those slight variations among the time constants which preserve their sum, but which alter the fastest time constant, result in considerable worsening of the fit of the model to the peaks in the transfer function data.

The determination of the strength of the self-inhibitory process is quite straightforward, and the parameter is thus fixed with considerable accuracy.

The time constant is less strongly reflected in the computations, and is thus less rigidly determined. It may also be noted that we have determined the effective parameters of the combined effect of self-inhibitory transients and the encoder transduction. Thus, our values for these parameters are, to some extent, also a function of our choice of encoder model (see Appendix).

The Fourier synthesis comparisons further enhance our confidence in the model. However, in general, they are less sensitive to the choice of parameters than are the Bode plots or reciprocal loci, because they constitute, in effect, averages over a large number of spatiotemporal frequencies.

Our choice for the parameters of the Hartline-Ratliff model may be compared with those determined by more direct means in other studies (see Appendix). In general, the agreement is very good, considering our indirect methods, and the elevated temperature of our preparation, which considerably "speeds up" the time scale of the eye. Comparison of our measurements of the inhibitory kernel with other measurements is rather complex, and is discussed separately in the Appendix.

We thus conclude that the spatiotemporal transfer function provides a convenient and concise characterization of the dynamics of the *Limulus* retina. This characterization can be readily interpreted in terms of component processes of the visual transduction, and quantitative descriptions of these component transductions can be obtained from the transfer function data. The Hartline-Ratliff model summarizes this analysis, and provides good quantitative predictions of the integrated response of the eye. Similar analyses may be useful in the study of other linear biological systems.

APPENDIX

Comparison of Transfer Function Parameters with Direct Measurement

Most of the parameters of the Hartline-Ratliff model correspond to quantities which can be determined directly, or inferred, from more invasive measurements of *Limulus* retinal physiology than were performed for this study. While those experiments, by their nature, effectively preclude the simultaneous determination of all the parameters for a single preparation, as was possible in this study, and have rarely been performed on the eye *in situ*, it is nevertheless instructive to compare our parameter values with those obtained by other methods.

The major systematic difference between our parameters and those obtained previously is that most of our time constants are faster, often by a factor of 2 or more. This is most likely a consequence of the fact that our data were obtained from *in situ* eyes at a temperature of approximately 22°C. At such an elevated temperature, most processes within the eye appear to run faster than they do at lower temperatures (Brodie, 1978). For example, our data show a peak response to flickering light at about 6 Hz, in contrast to values around 3 Hz previously reported in colder, excised eyes (Knight, 1973 *a*).

We consider first the parameters for the generator potential. These describe properties of the discrete bumps which sum to form the observed potential.

The most complete measurements of these parameters, from intracellular votlage data, are those of Wong (1977). (Many other measurements of bump parameters have been made at much lower light levels than the present experiments. Such conditions facilitate the study of individual bumps, but they also obscure the adaptation effect and

lengthen the latency between photon absorption and the consequent bump.) His parameter values (for excised eyes) were $t_l = 0.025$ s, 20°C, $Q_{10} = 4$; $t_d = 0.016$ s, 20°C, $Q_{10} = 4$; $n_d = 3$; $t_b = 0.03$ s, 20°C, $Q_{10} = 2.5$; $n_b = 3$; $R = 0.59$; $t_a = 0.074$ s (temperature dependence not measured). Comparison with Table II shows reasonable agreement, though comparison of the time constants is somewhat complicated by the difference in the exponents n_d and n_b. Wong did not measure the temperature dependence of the adaptation parameters. Nonetheless, even if we assume that the time constant t_a varies with temperature in a manner similar to the other time constants, our data show an adaptation process considerably faster, and slightly stronger, than that described by his measurements.

It may also be noted that our value of eight for the number of factors of the form $1/(1 + i\omega t)$ in our model for the generator potential is in good agreement with the original estimates of Fuortes and Hodgkin (1964). Under conditions of strong light adaptation, their estimates of the number apparent of "stages" of filtering in the generator potential ranged from 7 to 13, with a mean of 10.1.

The encoder parameters describe the strength and time scale of the self-inhibitory process. This process has been studied in excised eyes (Stevens, 1964; Purple, 1964; Lange, 1965; Knight et al., 1970; Fohlmeister et al., 1977 *b*) and in *in situ* preparations (Biederman-Thorson and Thorson, 1971). These numerous studies give self-inhibitory parameters which vary widely: $\kappa = 1.$ to $\kappa = 6.$; $\tau = 0.250$ to $\tau = 1.0$ s. Our data (Table II) are compatible with the faster and weaker ends of this range. Our rapid time constant may be due to the elevated temperature of our preparations. It should also be noted that our treatment assigns an effective time constant only to the combined processes of self-inhibition and impulse generation. It is possible that the impulse-generating process (which is in fact better described by a "forgetful" integrate-and-fire mechanism than by the simple model given above) contributes a high-pass characteristic of its own to the dynamic response of the eye. As "forgetting" time constants for the *Limulus* eccentric cell have been reported ranging from 0.04 s to < 0.01 s (Barbi et al., 1975; Fohlmeister et al., 1977 *b*), our apparent time constant for the complete encoder might well be faster than the actual time constant of the intracellular self-inhibitory hyperpolarization. In any event, except for the slow component of light adaptation, self-inhibition is clearly the slowest process in our model of the *Limulus* eye.

The parameters for the temporal dependence of lateral inhibition seldom have been measured directly. The impulse responses measured by Knight et. al. (1970) were approximated by them with the following (unpublished) parameter values: $\tau_1 = 0.1$ s, $\tau_2 = 0.15$ s, $\tau_3 = 0.1$ s, $\tau_4 = 0.05$ s, $C = 0.1$. Our time constants (Table II) are faster by a factor of 3, but are still reasonable. The vanishing of the constant C for one of our preparations is consistent with results observed in nonhyperpolarized cells. Clearly, most of the effective "delay" of the inhibitory treatment is accounted for by the three low-pass filter stages.

Previous measurements of the inhibitory kernel have been made in excised eyes (using steady-state data) by Kirschfeld and Reichardt (1964); Barlow (1967, 1969); and Johnston and Wachtel (1976), all using very different methods. Kirschfeld and Reichardt measured steady-state Mach bands, and modeled their data with kernels given by the forms $k(x) = Ae^{-|x|/a}$ and $k(x) = Ae^{-x^2/a^2}$. They assumed a priori that the kernel decreased monotonically away from the origin. They were able to rule out the simple exponential kernel, and found that their data were adequately described by the Gaussian kernel, with a space constant $a = 0.22$ eye widths. This is in good agreement with our measured value. It should be noted, however, that the observed Mach band patterns are in fact rather insensitive to the details of the inhibitory kernel, especially as regards detection of a small crater in the inhibitory field (Barlow and Quarles, 1975).

Barlow directly measured the point-to-point inhibitory coupling of single units to small clusters of inhibiting ommatidia. He obtained a two-dimensional inhibitory field with a marked central crater. Johnston and Wachtel's measurements were performed on eyes with the cornea and crystalline cones removed. They obtained a monotonically decreasing inhibitory kernel extending to about 0.25 eye widths from the test ommatidium.

Dodge and Kaplan (1975)[7] measured the inhibitory fields of the *in-situ Limulus* eye by measuring the response to flashing bars as viewed on a screen 10. cm from the eye by the *Limulus* using its natural optics in air. Their data were basically in agreement with previous investigators; they found a narrow crater in one-third of their units.

In order to compare our one-dimensional data with these various measurements, it is necessary to consider the relationship between the two-dimensional kernel and our one-dimensional treatment. If one illuminates the entire eye, and assumes that, for a centrally located ommatidium, the top and bottom edges of the eyes are (effectively) infinitely far away, then the two-dimensional Hartline-Ratliff equations (Eq. 6) may be replaced by a one-dimensional analog in which the inhibitory kernel is simply related to its two-dimensional counterpart:

$$k(x) = \int_{-\infty}^{\infty} k(x,y)\mathrm{d}y. \tag{A1}$$

If the illumination pattern covers only a finite strip of the eye, the simple relation (Eq. A1) will no longer hold. Instead we have

$$k(x) = \int_{-Y}^{Y} k(x,y)g(y)\mathrm{d}y/g(0), \tag{A2}$$

where the illumination strip spans the region from $-Y$ to Y, and $g(y)$ is the steady-state response of an ommatidium at the distance y from the x-axis to the analysis stimulus consisting of a uniform bar of light ($\xi = 0$). (We have not attempted to measure the weighting function $g(y)$, but the edge effects measured elsewhere (Barlow and Quarles, 1975; Kirschfeld and Reichardt, 1964) suggest that taking g to be a constant function of y should be an adequate approximation.) When the two-dimensional kernel of Eq. 16 is inserted in Eq. A2, we may observe several facts. First, the integral takes the form of a sum of two terms, each of which is a function of x times the integral of a function of y. This implies that the space-constants a and b determined for the one-dimensional kernel are the same as the space constants of the two-dimensional kernel. Second, the ratio B/A of the two components of the one-dimensional kernel is related to the analogous ratio (D in Eq. 16) of the two-dimensional kernel by the relation:

$$\frac{B}{A} = D \cdot \frac{\zeta b}{\eta a} \cdot \frac{\mathrm{erf}(Y/\zeta b)}{\mathrm{erf}(Y/\eta a)}, \tag{A3}$$

where $\mathrm{erf}(u) \equiv \int_0^u e^{-v^2}dv$.

We distinguish two limiting cases: if Y is large (compared to ηa) then the error function quotient is approximately unity, and we see that the "apparent" crater strength B/A is less than the actual strength D by a factor of $\zeta b/\eta a$; in other words, the crater is "filled in" by the integration over y. If Y is small (compared to ζb), then $\mathrm{erf}(Y/\zeta b) \cong Y/\zeta b$ (and likewise for $\mathrm{erf}[Y/\eta a]$), and the observed quotient B/A is equal to the true crater strength D. Our experiment falls between these two limits, with $Y = 0.0666$ eye widths, $\eta a = 0.09$ eye widths and $\zeta b = 0.02$ eye widths. This gives $D = (B/A)\cdot 3.1 = 1.8$. Although this number, if taken at face value, suggests that the two-dimensional kernel actually takes on negative

[7] Dodge, F. A., and E. Kaplan. Personal communication.

values, it must be remembered that this value for D results from the product of the observed ratio A/B and the square of the ratio $(\zeta b/\eta a)$ of two very small and somewhat crudely estimated parameters. It is also to be noted that, for such small features of the inhibitory kernel as the crater, the continuous model of the *Limulus* retina breaks down, in that it tries to describe features whose scale is comparable to the size of a single ommatidium. Nonetheless, similar observations from several preparations allow us to conclude that the crater depth parameter D is approximately unity, a value compatible with Barlow's data.

Our value for the space constant, a, of the main feature in the inhibitory kernel in the horizontal direction is in good agreement with all the previous measurements, in which the kernel falls to zero at around 0.25 eye widths from the test ommatidium. Our value for the space constant, b, of the crater corresponds to a feature about one-half as wide as that described by Barlow. Such a narrow feature would be difficult to detect with methods which produce a wider point-spread effect than our fiber-optic taper arrangement. In the vertical direction, our space constant, a, was about one-half of that in the horizontal direction, a ratio comparable to Barlow's measurements. Our value for the space constant of the crater in the vertical direction was only slightly less than the value in the horizontal direction, though, as mentioned above, the width of the crater is one of our least well determined parameters. These ratios must also be evaluated in light of the fact that they derive from measurements of different *Limulus* specimens.

The width of the stimulus stripe also enters into the comparison of our value for $\mathbf{K}$ with previous measurements. (Actually, the relevant parameter is the quotient $\mathbf{K}/(1 + \kappa)$, which is equivalent to the sum of the inhibitory coefficients in steady-state experiments.) We have

$$\mathbf{K} = \int_{-\infty}^{\infty} k(x)\mathrm{d}x = \int_{-\infty}^{\infty}\int_{-Y}^{Y} k(x, y)g(y)\mathrm{d}y\mathrm{d}x/g(0). \tag{A4}$$

For our present purposes, we set g equal to a constant; furthermore, we may ignore the crater in this comparison, as it alters the total inhibitory strength by only $\sim 2\%$. With these approximations, inserting our values for Y and ηa in Eq. A4 yields the conclusion that our value for $\mathbf{K}/(1 + \kappa)$ is $\sim 70\%$ of the total steady-state inhibitory strength of the whole eye.

Barlow (1967) stated that the sum of the coefficients in his inhibitory kernel was 7, though this is a considerable extrapolation which probably overrepresents the ommatidia with atypically strong inhibitory coupling. Lange (1965) gave values as large as 2. In their subsequent paper Barlow and Lange (1974) emphasized the dependence of the total inhibitory strength on the level of excitation of the ommatidium being inhibited. They reported values for this parameter which varied (in different preparations) from 0.4 to 2.3, all for an excitation of 25 impulses/s; in one preparation, they measured a total inhibition of 0.6 at an excitation of 5 impulses/s, rising linearly to 1.7 at an excitation of 20 impulses/s.

Our experimental design does not permit direct measurement of the excitation level of our test ommatidium, but we may estimate the excitation from the steady-state relation

$$r = e/\left(1 + \frac{\mathbf{K}}{1 + \kappa}\right). \tag{A5}$$

Inserting the observed mean impulse rate $r = 10$ impulses/s, and inhibitory strength $\mathbf{K}/(1 + \kappa) = 1.3$, we recover the estimate $e = 23$ impulses/s. Thus, our corrected value for the inhibitory strength of the entire eye, $\mathbf{K}/(1 + \kappa)$ (whole eye) $= 1.3/0.7 = 1.9$, is in excellent agreement with the measurements of Barlow and Lange. Kirschfeld and Reichardt (1964) found a total inhibitory strength of 1.111, at an excitation of over 30

impulses/s. Recently, Barlow and Fraioli (1978) have obtained values for $\mathbf{K}/(1 + \kappa)$ ranging from 1.5 to 3.7, for excitations comparable to ours. They report that the strength of lateral inhibition appears greatest in those animals in the best physiological condition.

Finally, though the effective point-spread characteristic of our optical system has little consequence for the natural optics of the *Limulus* eye, it compares favorably with the point-spread functions measured for a *Limulus* ommatidium in air and in water by Kirschfeld and Reichardt (1964), whose data were summarized by Gaussian distributions with s-parameters of approximately 0.019.

This work was supported, in part, by grants EY 188, EY 1428, EY 1472, and GM 1789 from the National Institutes of Health.

Received for publication 5 January 1977.

REFERENCES

BARBI, M., V. CARELLI, C. FREDIANI, and D. PETRACCHI. 1975. The self-inhibited leaky integrator: transfer functions and steady state relations. *Biol. Cybern.* **20**:51–59.

BARLOW, R. B., JR. 1967. Inhibitory fields in the *Limulus* lateral eye. Thesis. The Rockefeller University, New York.

BARLOW, R. B., JR. 1969. Inhibitory fields in the *Limulus* lateral eye. *J. Gen. Physiol.* **54**:383–396.

BARLOW, R. B., JR., and G. D. LANGE. 1974. A nonlinearity in the inhibitory interactions in the lateral eye of *Limulus*. *J. Gen. Physiol.* **63**:579–589.

BARLOW, R. B., JR., and D. A. QUARLES. 1975. Mach bands in the lateral eye of *Limulus*. Comparison of theory and experiment. *J. Gen. Physiol.* **65**:709–730.

BARLOW, R. B., JR., and A. J. FRAIOLI. 1978. Inhibition in the *Limulus* lateral eye *in situ*. *J. Gen. Physiol.* **71**:699–720.

BIEDERMAN-THORSON, M., and J. THORSON. 1971. Dynamics of excitation and inhibition in the light-adapted *Limulus* eye *in situ*. *J. Gen. Physiol.* **58**:1–19.

BRODIE, S. E. 1978. Temperature dependence of the dynamic response of the *Limulus* retina. *Vision Res.* In press.

BRODIE, S. E., B. W. KNIGHT, and F. RATLIFF. 1978. The response of the *Limulus* retina to moving stimuli. A prediction by Fourier synthesis. *J. Gen. Physiol.* **72**:000–000.

DODGE, F. A. 1969. Inhibition and excitation in the *Limulus* eye. *In* Processing of Optical Data by Organisms and by Machines. Proceedings of the International School of Physics "Enrico Fermi," Course XLIII. W. Reichardt, editor, Academic Press, Inc.,New York. 341–365.

DODGE, F. A., and E. KAPLAN. 1975. Visual fields in the *Limulus* eye. *Biophys. J.* **15**:172*a*. (Abstr.)

DODGE, F. A., B. W. KNIGHT, and J. TOYODA. 1968. Voltage noise in *Limulus* visual cells. *Science* (*Wash. D.C.*). **160**:88–90.

FOHLMEISTER, J. F., R. E. POPPELE, and R. L. PURPLE. 1977 *a*. Repetitive firing: a quantitative study of feedback in model encoders. *J. Gen. Physiol.* **69**:815–848.

FOHLMEISTER, J. F., R. E. POPPELE, and R. L. PURPLE. 1977 *b*. Repetitive firing: quantitative analysis of encoder behavior of slowly adapting stretch receptor of crayfish and eccentric cell of *Limulus*. *J. Gen. Physiol.* **69**:849–877.

FUORTES, M. G. F., and A. L. HODGKIN. 1964. Changes in time scale and sensitivity in the ommatidia of *Limulus*. *J. Physiol.* (*Lond.*). **172**:239–263.

GRAHAM, N., and F. RATLIFF. 1974. Quantitative theories of the integrative action of the retina. *In* Contemporary Developments in Mathematical Psychology. D. H. Krantz, R. C. Atkinson, R. D. Luce, and P. Suppes, editors. W. H. Freeman & Co., San Francisco. **2**:306–371.

HARTLINE, H. K., and C. H. GRAHAM. 1932. Nerve impulses from single receptors in the eye. *J. Cell. Comp. Physiol.* **1**:227–295.

HARTLINE, H. K., and F. RATLIFF. 1957. Inhibitory interaction of receptors units in the eye of *Limulus*. *J. Gen. Physiol.* **40**:357–376.

HARTLINE, H. K., and F. RATLIFF. 1958. Spatial summation of inhibitory influences in the eye of *Limulus*, and the mutual interaction of receptor units. *J. Gen. Physiol.* **41**:1049–1066.

JOHNSTON, D., and H. WACHTEL. 1976. Electrophysiological basis for the spatial dependence of the inhibitory coupling in the Limulus retina. *J. Gen. Physiol.* **67**:1–25.

KIRSCHFELD, K., and W. REICHARDT. 1964. Die Verarbeitung stationärer optischer Nachrichten im Komplexauge von Limulus. (Ommatidien-Sehfeld und räumliche Verteilung der Inhibition). *Kybernetik*. **2**:43–61.

KNIGHT, B. W. 1972. Dynamics of encoding in a population of neurons. *J. Gen. Physiol.* **59**:734–766.

KNIGHT, B. W. 1973 *a*. The horseshoe crab eye: a little nervous system that is solvable. *In* Lectures on Mathematics in the Life Sciences. Some Mathematical Questions in Biology, IV. J. B. Cowan, editor. The American Mathematical Society, Providence, R. I. **5**:113–144.

KNIGHT, B. W. 1973 *b*. Some questions concerning the encoding dynamics of neuron populations. *In* Communication and Control Processes in Biological Systems. International Union for Pure and Applied Biophysics, Academy of Sciences of the U.S.S.R., Symposial Papers. 422–436.

KNIGHT, B. W. 1973 *c*. A stochastic problem in visual neurophysiology. *In* Stochastic Differential Equations: Society for Industrial and Applied Mathematics-American Mathematical Society Proceedings. J. B. Keller and H. P. McKean, editors. American Mathematical Society, Providence, R. I. **6**:1–19.

KNIGHT, B. W. 1977. Modelling the Dynamics of the Retina. *In* Spatial Contrast: Report of a Workshop Held in Amsterdam, 4–9 January 1976. H. Spekreijse and L. H. Van der Tweel, editors. North-Holland Publishing Co., Amsterdam. 120–124.

KNIGHT, B. W., J. TOYODA, and F. A. DODGE. 1970. A quantitative description of the dynamics of excitation and inhibition in the eye of Limulus. *J. Gen. Physiol.* **56**:421–437.

LANGE, G. D. 1965. Dynamics of inhibitory interactions in the eye of *Limulus*: experimental and theoretical studies. Thesis. The Rockefeller Institute, New York.

LEUNG, L. S., and W. J. FREEMAN, 1977. The spatial temporal response of the *Limulus* eye neural set. *J. Theor. Biol.* **69**:41–56.

PINTER, R. B. 1966. Sinusoidal and delta function responses of visual cells of the *Limulus* eye. *J. Gen. Physiol.* **49**:565–593.

PURPLE, R. L. 1964. The integration of excitatory and inhibitory influences in the eccentric cell in the eye of *Limulus*. Thesis. The Rockefeller Institute, New York.

RATLIFF, F., editor. 1974. Studies on Excitation and Inhibition in the Retina. The Rockefeller University Press, New York.

RATLIFF, F., B. W., KNIGHT, F. A. DODGE, and H. K. HARTLINE. 1974. Fourier analysis of dynamics of excitation and inhibition in the eye of *Limulus*: amplitude, phase, and distance. *Vision Res.* **14**:1155–1168.

RATLIFF, F., B.W. KNIGHT, and N. GRAHAM. 1969. On tuning and amplification by lateral inhibition. *Proc. Natl. Acad. Sci. U. S. A.* **62**:733–740.

RATLIFF, F., B. W. KNIGHT, and N. MILKMAN. 1970. Superposition of excitatory and inhibitory influences in the retina of *Limulus*: effect of delayed inhibition. *Proc. Natl. Acad. Sci. U. S. A.* **67**:1558–1564.

RATLIFF, F., B. W. KNIGHT, J. TOYODA, and H. K. HARTLINE. 1967. Enhancement of flicker by lateral inhibition. *Science (Wash. D.C.)*. **158**:392–393.

RUSHTON, W. A. H. 1961. The intensity factor in vision. *In* A Symposium on Light and Life. W. D. McElroy and B. Glass, editors. The Johns Hopkins Press, Baltimore. 706–723.

SHAPLEY, R. M. 1971. Effects of lateral inhibition on fluctuations of the impulse rate. *J. Gen. Physiol.* **57**:557–575.

STEVENS, C. F. 1964. A quantitative theory of neural interactions: theoretical and experimental investigations. Thesis. The Rockefeller Institute, New York.

THORSON, J., and M. BIEDERMAN-THORSON. 1974. Distributed relaxation processes in sensory adaptation. *Science (Wash. D.C.)*. **183**:161–172.

VICTOR, J. D., R. M. SHAPLEY, and B. W. KNIGHT. 1977. Nonlinear analysis of cat retinal ganglion cells in the frequency domain. *Proc. Natl. Acad. Sci. U. S. A.* **74**:3068–3072.

WONG, F. 1977. Mechanisms of the phototransduction process in invertebrate photoreceptors. Thesis. The Rockefeller University, New York.